UPPSALA
UNIVERSITET

Digital Comprehensive Summaries of Uppsala Dissertations from the Faculty of Science and Technology 1536

Joint inversion and integration of multiple geophysical data for improved models of near-surface structures

SHUNGUO WANG

ACTA
UNIVERSITATIS
UPSALIENSIS
UPPSALA
2017

ISSN 1651-6214
ISBN 978-91-513-0018-4
urn:nbn:se:uu:diva-327096

Dissertation presented at Uppsala University to be publicly examined in Hambergsalen, Villavägen 16, Uppsala, Monday, 18 September 2017 at 10:00 for the degree of Doctor of Philosophy. The examination will be conducted in English. Faculty examiner: Professor Mark Everett (Texas A&M University, Department of Geology and Geophysics).

Abstract

Wang, S. 2017. Joint inversion and integration of multiple geophysical data for improved models of near-surface structures. *Digital Comprehensive Summaries of Uppsala Dissertations from the Faculty of Science and Technology* 1536. 65 pp. Uppsala: Acta Universitatis Upsaliensis. ISBN 978-91-513-0018-4.

Geophysical methods are non-invasive and allow an effective way of understanding subsurface structures and their physical properties. One of the main challenges is the often non-uniqueness of the geophysical models and that several different models can explain a dataset to an agreeable fit. Moreover, noise and limitations in resolution, which are inherent to field data, are additional obstacles for obtaining a true physical property model of the subsurface. Facing all these challenges, geophysicists have dedicated their efforts for decades to recover models that represent, as close as possible, the true subsurface. Joint inversion and integration of multiple geophysical data are two main approaches that I studied to better resolve subsurface structures. I further used these approaches, together with new software and hardware implementations for data acquisition and inversion, for near-surface applications.

In this thesis, radio-magnetotelluric (RMT), boat-towed RMT, boat-towed controlled source MT (CSMT), electrical resistivity tomography (ERT), and first-arrival traveltime tomography are jointly used for quick clay investigations and fracture zone delineation under shallow water-bodies. The joint approach, as compared with any individual method, shows a better ability to both resolve the geological targets and to assist in understanding the subsurface geology that hosts these targets. For examples: by performing the joint inversion of lake-floor ERT and boat-towed RMT data, a fracture zone is better delineated with greater details compared with single inversion; by employing boat-towed CSMT measurements and jointly inverting with boat-towed RMT data, the subsurface structures, especially at greater depth, are better resolved than by inverting each dataset alone.

During my PhD studies, two types of new implementations were employed. (1) Boat-towed data acquisition system was implemented to expand the RMT and CSMT method from land to shallow-water applications. This is significant since many large-scale underground infrastructures are likely to cross these water zones (for example multi-lane train or bypass tunnels, such as the Stockholm bypass). (2) The modification of a well-structured code EMILIA allows joint inversion of boat-towed RMT and lake-floor ERT datasets, and the modification of another well-structured code MARE2DEM can accurately model high frequency CSMT data and handle joint inversion of boat-towed RMT and boat-towed CSMT datasets. Thus, the code modification as another type of new implementation guarantees the success of near-surface applications using the boat-towed RMT and CSMT data acquisition systems.

Studies conducted during my PhD work, included under the SEG-GWB (the Society of Exploration Geophysicists - Geoscientists *Without* Borders) program and the TRUST (TRansparent Underground STructure) umbrella project, are useful for near-surface applications including, for examples, engineering purposes such as planning of underground infrastructures, site characterization in connection with energy or waste storage, and geohazard investigations.

Keywords: joint inversion, ERT, RMT, CSRMT, boat-towed, tomography

Shunguo Wang, Department of Earth Sciences, Geophysics, Villav. 16, Uppsala University, SE-75236 Uppsala, Sweden.

ISSN 1651-6214
ISBN 978-91-513-0018-4
urn:nbn:se:uu:diva-327096 (http://urn.kb.se/resolve?urn=urn:nbn:se:uu:diva-327096)

Dedicated to my family

谨以此文献给我的家人

Supervisors & Examination Committee

Supervisors

Professor Alireza Malehmir
Department of Earth Sciences, Uppsala University, Uppsala, Sweden

Dr. Mehrdad Bastani
Geological Survey of Sweden, Uppsala, Sweden

Associate Professor Thomas Kalscheuer
Department of Earth Sciences, Uppsala University, Uppsala, Sweden

Faculty Opponent

Professor Mark Everett
Department of Geology and Geophysics, Texas A&M University, College Station, USA

Examination Committee

Professor Bülent Tezkan
Institute of Geophysics and Meteorology, University of Cologne, Cologne, Germany

Dr. Ute Weckmann
GFZ German Research Centre for Geosciences, Helmholtz Centre Potsdam, Potsdam, Germany

Senior Lecturer Ari Tryggvason
Department of Earth Sciences, Uppsala University, Uppsala, Sweden

Dr. Gerhard Schwarz (reserve)
Geological Survey of Sweden, Uppsala, Sweden

List of papers

This thesis is based on the following papers, which are referred to in the text by their Roman numerals.

I **Wang, S.**, Malehmir, A. and Bastani, M., 2016. Geophysical characterization of areas prone to quick-clay landslides using radio-magnetotelluric and seismic methods. *Tectonophysics*, 677, 248-260.

II **Wang, S.**, Kalscheuer, T., Bastani, M., Malehmir, A., Pedersen, L.B., Dahlin, T. and Meqbel N., 2017. Joint inversion of lake-floor electrical resistivity tomography and boat-towed radio-magnetotelluric data illustrated on synthetic data and an application from the Äspö Hard Rock Laboratory site, Sweden. *Geophys. J. Int.* (under revision).

III **Wang, S.**, Bastani, M., Constable, S., Kalscheuer, T., and Malehmir, A., 2017. Using boat-towed controlled source radio-magnetotelluric data to resolve fracture zones at Äspö Hard Rock Laboratory site, Sweden. *Manuscript*.

Reprints were made with permission from the publishers.

Selected publications during my PhD study which are not included into this thesis.

I Malehmir, A., **Wang, S.**, Lamminen, J., Brodic, B., Bastani, M., Vaittinen, K., Juhlin, C., Place, J., 2015. Delineating structures controlling sandstone-hosted base-metal deposits using high-resolution multicomponent seismic and radio-magnetotelluric methods: a case study from Northern Sweden. *Geophys. Prospect.*, **63**(4), 774-797.

II **Wang, S.**, Bastani, M., Kalscheuer, T., Malehmir, A., Dynesius, L., 2017. Controlled source boattowed radio-magnetotellurics for site investigation at Äspö Hard Rock Laboratory, southeastern Sweden. *79th EAGE Conference and Exhibition*, Paris, France.

III **Wang, S.**, Kalscheuer, T., Bastani, M., Malehmir, A., Pedersen, L.B., Dahlin, T., Meqbel, N., 2016. Joint inversion of on-lake radio-magnetotelluric and lake-floor direct current resistivity data and its applications. *23rd EM Induction Workshop*, Chiang Mai, Thailand.

IV **Wang, S.**, Bastani, M., Malehmir, A., 2014. Integrated use of radio-magnetotelluric and high-resolution reflection seismic data to delineate near surface structures – two case studies from Sweden. *22nd EM Induction Workshop*, Weimar, Germany.

Contents

Abbreviations

1D	One-Dimensional
2D	Two-Dimensional
2.5D	Three-Dimensional Source and Two-Dimensional Subsurface
3D	Three-Dimensional
BH	Borehole
CSEM	Controlled Source Electromagnetics
CSMT	Controlled Source Magnetotellurics
CSRMT	Controlled Source Radio-Magnetotellurics
DGPS	Differential Global Positioning System
EM	Electromagnetics
EMILIA	Electro-Magnetic Inversion using Least Intricate Algorithms
ERT	Electrical Resistivity Tomography
FDM	Finite Difference Method
FEM	Finite Element Method
GPR	Ground Penetrating Radar
HRL	Hard Rock Laboratory
MARE2DEM	Modelling with Adaptively Refined Elements for 2D Electromagnetics
PDE	Partial Differential Equation
RMS	Root Mean Square
RMT	Radio-Magnetotellurics
SGU	Geological Survey of Sweden
SIO	Scripps Institution of Oceanography
SKB	Swedish Nuclear Fuel and Waste Management Company
S/N	Signal-to-Noise Ratio
TE	Transverse Electric
TM	Transverse Magnetic
UU	Uppsala University
VLF	Very Low Frequency
VMT	Vertical Magnetic Transfer Function

1 Introduction

It is well known that geophysical inverse problems suffer from non-linearity and ill-posedness, and finding a unique model fitting one geophysical dataset is an extremely difficult task. Joint inversion and integration of multi-geophysical data, however, are useful techniques to narrow down the range of models that can properly represent the data. In this thesis, these techniques have been used with different geophysical datasets, such as apparent resistivity, resistance, and travel time, for better modelling near-surface structures and their physical properties. The objective of my research is mainly to improve the resolution of geophysical data in near-surface applications.

For the integration strategy, separate inversions or data processing of individual datasets can be carried out. Different and similar features in individual models are then combined for an improved interpretation of a geological target (or several) and to reduce uncertainty in the models. For the joint inversion with similar material property (e.g., resistivity), it is naturally coupled by inverting different datasets for the same property, for examples, among different types of electromagnetic (EM) data (e.g., Vozoff and Jupp, 1975; Candansayar and Tezkan, 2008; Kalscheuer et al., 2010, 2015) or among different types of seismic data (e.g., Julia et al., 2000; Tryggvason and Linde, 2006). For the joint inversion with two or more types of material properties, two coupling methods, direct parameter and cross-gradient couplings are mainly used (e.g., Moorkamp et al., 2011, 2016; Abubakar et al., 2012; Haber and Gazit, 2013). Direct parameter coupling is usually based on the information obtained using laboratory measurements of rock samples or downhole logging information and is possibly valid for a small part of the model (Lines et al., 1988; Coutant et al., 2012). Cross-gradient coupling is easier to implement, however, it is not as strong as the direct parameter one (e.g., Gallardo and Meju, 2003, 2004, 2007, 2011; Tryggvason and Linde, 2006; Hu et al., 2009; Moorkamp et al., 2010, 2016).

Radio-magnetotelluric (RMT), boat-towed RMT, boat-towed controlled source MT, electrical resistivity tomography (ERT), and first-arrival traveltime tomography are the main methods used in my thesis. Each method has its own advantages and disadvantages in resolving near-surface structures and their properties. For examples, the RMT method is good at resolving conductive materials and the data acquisition is efficient, fast and cost-effective. However, resolution and penetration of the method are limited when carried out on conductive sediments or over saline water-bodies. The

CSMT method has higher resolution at depth because it uses lower frequencies but the measurements require much longer time than the RMT method. The ERT method is not superior to resolve conductor, as compared with the RMT and CSMT methods, but it has better resolution for resolving resistive materials. Thus, integration and joint inversion of these different datasets aim to combine the advantages of different methods for an improved resolution and a more detailed delineation of targets. These approaches have been tested and evaluated in three near-surface applications and the results are shown in three papers that are included in the second part of the thesis. I provide a short summary of their objectives here.

In **Paper I**, RMT and first-arrival traveltime tomography are jointly integrated to map quick clays and their host structures. The study was conducted within a project under the SEG-GWB (SEG, 2017) program. Quick clays and related landslides in the Nordic countries and North America are among the most important geohazards that need to be carefully studied. The research area is located next to the Göta River in the south-western of Sweden. RMT results show that the resistivity of potential quick clays (10-100 ohm-m) is generally higher than the surrounding marine clays (1-10 ohm-m). The seismic tomography results show a relatively high-velocity feature associated with a combination of quick clays and underlying sand (or coarse-grained) layer. By the joint study of the RMT and seismic tomography results, combined with the seismic reflection results and calibration provided by boreholes, potential quick-clay zones were delineated and landslide scenarios were provided.

In **Paper II**, joint inversion of boat-towed RMT data and lake-floor ERT data is used to map fracture zones at Äspö Hard Rock Laboratory (HRL) in south-eastern Sweden. The study was conducted within the TRUST (TRUST, 2016) umbrella project, which aimed to improve the resolution of multi-geophysical data for near-surface applications, especially in urban environment. The boat-towed RMT data and lake-floor ERT data were jointly inverted through a modified inversion code EMILIA (Kalscheuer et al., 2010). The inverted resistivity model not only shows the known fracture zone, but also provides additional evidence for another fracture zone, which had only been inferred in previous studies. The results clearly demonstrate the advantage of using the new implementations of both data acquisition and inversion to improve resolution in near-surface applications.

In **Paper III**, joint inversion of boat-towed RMT and CSMT data is used to map the same fracture zones as in **Paper II**. 2D inversion of boat-towed CSRMT (including RMT and CSMT) data was separately done with EMILIA (Kalscheuer et al., 2008), which uses a plane-wave approximation for source effect, and with the modified MARE2DEM (Key, 2016), which fully considers the source effect. Compared with the results from EMILIA, the results from MARE2DEM suggest more features and potential fracture zones. The joint inversion of boat-towed RMT and CSMT data using MARE2DEM also reveals more detail of the fracture zones and bedrock

surface than any of the single inversions. In addition, this study also suggests that proper simulation should be done prior to acquisition to design an optimal observation system that minimizes the influence from the source effect.

This thesis is organized in six chapters. Chapter 1 introduces the objectives and methodologies of my research and gives a brief summary of the main results in the three papers. Chapter 2 gives a more in-depth presentation of the underlying theory of the used geophysical methods while chapter 3 presents the theory behind the inversion techniques involved, including Occam inversion and joint inversions. Chapter 4 presents more comprehensive summaries of the three papers to demonstrate the advantages of using joint inversion and integration of multi-geophysical datasets. Chapter 5 concludes the achievements that I have reached and suggests the potential continuation of my research. Finally, Chapter 6 contains a summary of the thesis in Swedish.

2 Theory of geophysical methods

2.1 Maxwell equations

The principle of electromagnetic (EM) methods can be described by Maxwell's equations. Equations 2.1-2.4 demonstrate the relationships between electric and magnetic fields for conduction and induction in the frequency domain with e^{iwt} as time dependency (Nabighian, 1987):

$$\nabla \times \mathbf{E} = -i\omega\mu\mathbf{H} - i\omega\mu\mathbf{M}_s , \tag{2.1}$$

$$\nabla \times \mathbf{H} = \left(i\omega\varepsilon + \sigma\right)\mathbf{E} + \mathbf{J}_s , \tag{2.2}$$

$$\nabla \cdot \mathbf{D} = \rho , \tag{2.3}$$

$$\nabla \cdot \mathbf{B} = 0 , \tag{2.4}$$

where in the international system (SI) of units, **D** (C/m^2) is the electric displacement, **B** (Wb/m^2) is the magnetic induction, **E** (V/m) is the electric field, **H** (A/m) is the magnetic field, $\mathbf{M}_s$ (A/m) is the magnetic current density of source, $\mathbf{J}_s$ (A/m^2) is the electric current density of source, ε (F/m) is the permittivity, σ (S/m) is the conductivity, μ (H/m) is the permeability, ω (Hz) is the angular frequency, and *i* represents imaginary unit.

The associated boundary conditions are governed by equation 2.5-2.6 (Nabighian, 1987):

$$\mathbf{n} \times \left(\mathbf{E}^1 - \mathbf{E}^2\right)\big|_\Gamma = 0 , \tag{2.5}$$

$$\mathbf{n} \times \left(\mathbf{H}^1 - \mathbf{H}^2\right)\big|_\Gamma = 0 , \tag{2.6}$$

where superscripts 1 and 2 indicate the fields in different medium, and **n** is the normal unit vector to the boundary between the two media.

In the case of radio-magnetotellurics (RMT) studies, the source components, $\mathbf{M}_s$ and $\mathbf{J}_s$, should be set to zero. However, in the case of controlled source radio-magnetotellurics (CSRMT) method, depending on the source type, the source components should be taken into account.

To solve equations 2.1-2.4, dimensionality plays an important role. For a 1D Earth model, the analytical solution of EM fields or impedance is available. For a 2D or 3D Earth model, numerical methods, such as finite-difference method (FDM) (e.g., Aiken et al., 1973; Dey and Morrison, 1979), finite element method (FEM) (e.g., Coggon, 1971; Xu, 1994), and integral equation (e.g., Hohmann, 1971), are utilized.

2.2 Radio-magnetotelluric method

2.2.1 Traditional RMT

RMT is a passive-source EM method. The sources of signal are distant radio transmitters operating in the frequency range of 14 kHz to 1 MHz (Turberg et al., 1994; Tezkan et al., 1996; Bastani, 2001; Bastani and Pedersen, 2001; Pedersen et al., 2006; Bastani et al., 2012). Usually the radio transmitters are assumed to be far enough away from the survey area so that their signals can be assumed as planar EM waves. By measuring these signals one can estimate electrical properties of the near-surface structures.

In the RMT data acquisition, three components of the magnetic field (H_x, H_y and H_z) and two horizontal components of the electric field (E_x and E_y) are measured simultaneously (Fig. 2.1). Data acquisition, using Uppsala University (UU) equipment, is carried out with the so-called Enviro-MT system (Fig. 2.1) developed by Bastani (2001). Impedance tensor **Z** in equation 2.7 demonstrates the relationship between electric and magnetic fields**:**

$$\begin{bmatrix} E_x \\ E_y \end{bmatrix} = \begin{bmatrix} Z_{xx} & Z_{xy} \\ Z_{yx} & Z_{yy} \end{bmatrix} \begin{bmatrix} H_x \\ H_y \end{bmatrix}, \tag{2.7}$$

and the vertical magnetic field and horizontal magnetic fields are related by the vertical magnetic transfer function (VMT) **T** using:

$$H_z = \begin{bmatrix} T_x & T_y \end{bmatrix} \begin{bmatrix} H_x \\ H_y \end{bmatrix}, \tag{2.8}$$

where x and y represent the observation directions in the Cartesian coordinate system. Z_{xx}, Z_{xy}, Z_{yx}, Z_{yy}, T_x, and T_y are complex-valued variables related to electric and magnetic fields and contain information about the near-surface structures.

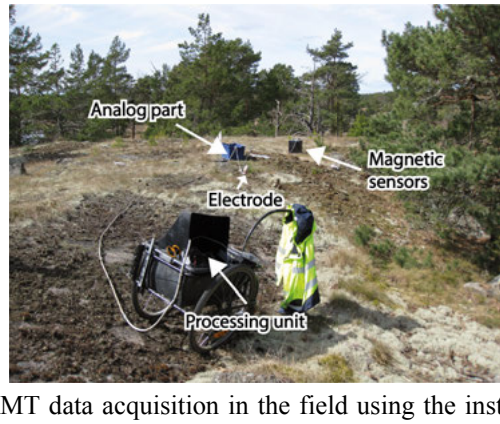

Figure 2.1. The RMT data acquisition in the field using the instrument Enviro-MT developed at UU (Bastani, 2001). The analog parts of the instrument, e.g., magnetic sensor and A/D converter, are positioned reasonably far from the processing unit. Photo: Mehrdad Bastani, 2015.

Apparent resistivity and phase of impedance at the surface of the Earth are defined as:

$$\rho_{xy/yx} = \frac{1}{\mu\omega}\left|Z_{xy/yx}\right|^2, \tag{2.9}$$

$$\varphi_{xy/yx} = \tan^{-1}\left(\frac{\mathrm{Im}\left(Z_{xy/yx}\right)}{\mathrm{Re}\left(Z_{xy/yx}\right)}\right), \tag{2.10}$$

where, x represents strike direction of the subsurface structures. Determinant impedance is defined as:

$$Z_{DET} = \sqrt{Z_{xx}Z_{yy} - Z_{xy}Z_{yx}}\ . \tag{2.11}$$

The elements of impedance tensor are determined by the primary field and the dimensionality of the near-surface structures. For a layered model with plane-wave as the primary field, the impedance tensor can be simplified to:

$$\begin{bmatrix} E_x \\ E_y \end{bmatrix} = \begin{bmatrix} 0 & Z_{xy} \\ -Z_{xy} & 0 \end{bmatrix}\begin{bmatrix} H_x \\ H_y \end{bmatrix}, \tag{2.12}$$

where the VMT function **T** vanishes.

For a 2D Earth model with plane-wave as the primary field, the impedance tensor can be simplified to:

$$\begin{bmatrix} E_x \\ E_y \end{bmatrix} = \begin{bmatrix} 0 & Z_{xy} \\ Z_{yx} & 0 \end{bmatrix}\begin{bmatrix} H_x \\ H_y \end{bmatrix}, \tag{2.13}$$

and the VMT function **T** is given as

$$H_z = \begin{bmatrix} 0 & T_y \end{bmatrix}\begin{bmatrix} H_x \\ H_y \end{bmatrix}. \tag{2.14}$$

where, Z_{xy} and Z_{yx} are defined as transverse electric (TE) mode and transverse magnetic (TM) mode, respectively. In areas where the strike direction is not clear, inversion of determinant impedance (equation 2.11) is more suitable to suppress 3D effects in 2D models than inversion of approximated TE or TM mode data (Pedersen and Engels, 2005).

For a 3D Earth model with plane-wave as the primary field, the impedance tensor and the VMT function have no simplification.

It is well known that the EM signal has a limited skin depth (Nabighian, 1987). The widely used skin depth is defined as:

$$\delta \approx 503\sqrt{\rho / f}\ , \tag{2.15}$$

where f is frequency (Hz). It is typically used to evaluate the maximal exploration depth at a given signal frequency as 1.5 δ (Spies, 1989). The resistivity ρ should be replaced by an effective resistivity $\tilde{\rho}$ in a layered medium (Spies, 1989; Huang, 2005).

2.2.2 Boat-towed RMT

Boat-towed RMT is a new method introduced by Bastani et al. (2015) for surveys over fresh and brackish water bodies. It originates from a land-based Enviro-MT acquisition system (Bastani, 2001). The difference between traditional RMT and boat-towed version is that the analog part of the Enviro-MT system is mounted on a floating frame made of wood and Styrofoam and towed by a boat instead of being carried physically by human (Fig. 2.2). The floating frame is at 10 m distance behind a boat and connected to the processing unit of the system positioned inside the boat (Fig. 2.2). Data acquisition with the boat-towed RMT is much more efficient than the land surveys due to the easy movment of the whole system with a boat after the setups are done. Later Mehta et al. (2017a) analyzed depth penetration of the method using synthetic examples and showed an applciation close to Stockholm city. Wang et al. (2017a) used the method together with lake-floor ERT to resolve fracture system under a saline water lake at Äspö hard rock laboratory (HRL) site in Sweden.

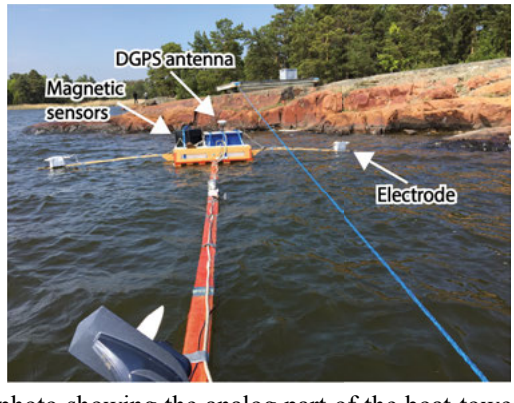

Figure 2.2. Field photo showing the analog part of the boat-towed RMT instrument is positioned on top of a floating frame and connected to the digital part via the white cable. The whole construction is towed behind a boat, which provides much faster acquisition speed compared with land-based measurements. The station coordinates can be recorded by a high-precision differential global positioning system (DGPS). In order to make the frame more stable, other means for example, a rope as shown in the figure can be used. Photo: Shunguo Wang, 2016.

2.2.3 Strike analysis

Field RMT data are usually collected along single profiles due to the time and financial limitations. The Earth, however, is 3D, thus, dimensionality and strike analysis of the RMT data is necessary. Using the estimated strike the data can be decomposed into TE and TM modes and later be inverted in 2D.

Determination of the strike of the dominant 2D geoelectrical structure from MT data is difficult in the presence of both noise and local distortions (Jones and Groom, 1993). A number of relevant publications discuss the strike rules for the MT impedance tensor in details (e.g., Swift, 1967; Zhang et al., 1987; Jones and Groom, 1993). In my studies, the method proposed by Zhang et al. (1987) is used for dimensionality and strike analysis. By doing this, independent strike angles can be found at each station and each frequency by minimizing the following function (Zhang et al., 1987):

$$Q = \left|\mathbf{Z}^*_{xx} - \beta \mathbf{Z}^*_{yx}\right|^2 + \left|\mathbf{Z}^*_{yy} - \gamma \mathbf{Z}^*_{xy}\right|^2, \tag{2.16}$$

where $\beta = \left(\tilde{\mathbf{Z}}^*_{xx} \cdot \mathbf{Z}^*_{yx}\right) / \left|\mathbf{Z}^*_{yx}\right|^2$, $\gamma = \left(\tilde{\mathbf{Z}}^*_{yy} \cdot \mathbf{Z}^*_{xy}\right) / \left|\mathbf{Z}^*_{xy}\right|^2$, a tilde and asterisk mean transposition and complex conjugation, and $\mathbf{Z}_{xx}$, $\mathbf{Z}_{xy}$, $\mathbf{Z}_{yx}$, and $\mathbf{Z}_{yy}$ are impedance tensor components over several adjacent frequencies and stations.

Well-designed field measurements based on available geological information can reduce the complexity of strike analysis. It may turn out that it is unnecessary to rotate the reference coordinate system to satisfy the requirement of the strike decomposition, moreover, this obviously is preferable.

2.2.4 Distortion parameters

When the regional EM fields are homogeneous across shallow distorters, the distorted impedance tensor $\mathbf{Z}$ and VMT functions (T_x T_y) are related to the undistorted impedance tensor $\mathbf{Z}^0$ and VMTs (T_x^0 T_y^0) through real-valued distortion parameters (Zhang et al., 1987; Groom and Bahr, 1992; Zhang et al., 1993; Kalscheuer et al., 2012):

$$\mathbf{Z} = \left(\mathbf{I} + \mathbf{P}_h\right)\mathbf{Z}^0\left(\mathbf{I} + \mathbf{Q}_h\mathbf{Z}^0\right)^{-1}, \tag{2.17}$$

$$\begin{pmatrix} T_x & T_y \end{pmatrix} = \left[\begin{pmatrix} T_x^0 & T_y^0 \end{pmatrix} + \mathbf{Q}_v\mathbf{Z}^0\right]\left(\mathbf{I} + \mathbf{Q}_h\mathbf{Z}^0\right)^{-1}, \tag{2.18}$$

where, $\mathbf{I}$ is the identity matrix, $\mathbf{P}_h$, $\mathbf{Q}_h$, and $\mathbf{Q}_v$ contain the distortion parameters of the horizontal electric field, the horizontal magnetic field, and the vertical magnetic field, respectively. The $\mathbf{P}_h$, $\mathbf{Q}_h$, and $\mathbf{Q}_v$ are defined as follows,

$$\mathbf{P}_h = \begin{pmatrix} P_{xx} & P_{xy} \\ P_{yx} & P_{yy} \end{pmatrix}, \tag{2.19}$$

$$\mathbf{Q}_h = \begin{pmatrix} Q_{xx} & Q_{xy} \\ Q_{yx} & Q_{yy} \end{pmatrix}, \tag{2.20}$$

$$\mathbf{Q}_v = \begin{pmatrix} Q_{zx} & Q_{zy} \end{pmatrix}. \tag{2.21}$$

The tensors $\mathbf{Q}_h$ and $\mathbf{Q}_v$ are frequency independent to galvanic distortion. The actual distortion effects on the magnetic fields, however, typically show frequency dependency (Kalscheuer et al., 2012).

2.3 Controlled source RMT

RMT data acquisition is rather convenient in the field, however, the RMT signal sources are not controlled by the operator during the measurements. Moreover the lowest frequency of 14 kHz in VLF band has a limited penetration depth especially over areas with extremely low resistivity. It is therefore recommended to use CSMT at lower frequencies. The method offers reasonably high signal-to-noise ratio (S/N) that is particularly suitable for resolving deeper subsurface targets in urban environment. The method was originally proposed by Goldstein and Strangway (1975).

The instrument Enviro-MT (Bastani, 2001) offers possibility of simultaneous measurements with RMT and CSMT methods (CSRMT in short term, Pedersen et al., 2005). The source can be remotely controlled by the operator at the receiver site using a radio modem. The available source frequencies are limited to 1, 1.25, 2, 2.25, 4, 6, 6.25, 8, 10, and 12.5 kHz. The selection of the frequencies depends on the target depth, resistivity of the subsurface, and background noise level.

Controlled source boat-towed RMT expands its application to previously limited field for boat-towed RMT in order to map subsurface structures. In the boat-towed CSRMT data acquisition (Fig. 2.3), a double horizontal magnetic dipole source is placed either on land or on the surface of water with a floating frame (possibly in the near future). Receiver part is the same as the

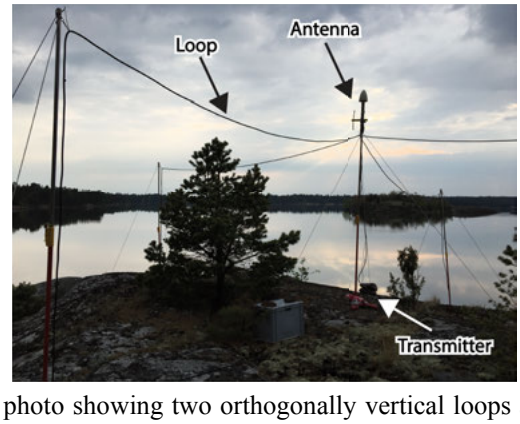

Figure 2.3. Field photo showing two orthogonally vertical loops are used as source for CSRMT measurements. With the current in the loops horizontal magnetic dipoles are formed. Besides, electrical source can also be used to transmit signals. The signal generator can be powered up by three 12 V car batteries. Photo: Shunguo Wang, 2016.

boat-towed RMT mounted on a floating frame and towed behind the boat (Bastani et al., 2015; Mehta et al., 2017a, 2017b; Wang et al., 2017a, 2017b). When the controlled source and receiver are set up and the boat is stable, the controlled source emits the signals at the frequencies selected by the operator. The receiver is then moved on the water after each station acquisition (the controlled source can also be moved if necessary) and a CSRMT profile is measured quite efficiently.

No matter how complex the subsurface media are, the controlled source usually generates data containing five components of EM fields with high S/N ratio. Thus, the measured fields can be directly used for inverting resistivity models of the subsurface. However, with the available boat-towed CSRMT system (Fig. 2.3), the controlled source current during the data acquisition cannot be recorded. Therefore, only the impedance tensor and VMT function are usable for inversion process.

2.4 Electrical resistivity tomography

The ERT method has been used for hydrogeological, mining, and geohazard investigations since 1939 in near-surface geophysics (Schlumberger, 1939; Daily et al., 2005).

In the ERT measurements, a direct current (I) is injected into the ground using a pair of electrodes, and a voltage (V) induced by the current is measured across another pair of electrodes (Fig. 2.4). In the ERT surveys, the Wenner (Fig. 2.4a), dipole-dipole (Fig. 2.4b), Schlumberger, and gradient electrode configurations are commonly used (Dahlin and Zhou, 2006).

The voltage in subsurface is subjected to partial differential equation (PDE):

$$\nabla \cdot \nabla V = -I_A \delta\left(r - r_A\right) - I_B \delta\left(r - r_B\right), \tag{2.22}$$

where V is the measured voltage, ∇ is the differential operator, δ is delta function which represents the source, and its position is represented by r_A and r_B. I_A and I_B represent the currents injected through electrodes A and B (Fig. 2.4), respectively. The ERT data are presented as pseudo-sections of apparent resistivity or resistance defined as:

$$\rho_a = k\frac{V}{I}, \tag{2.23}$$

or

$$R = \frac{V}{I}, \tag{2.24}$$

where k represents a geometric factor depending on the array type and electrode spacing. The resistivity measured by the ERT method can be considered as geometrically weighted average of the true resistivity distribution of the subsurface.

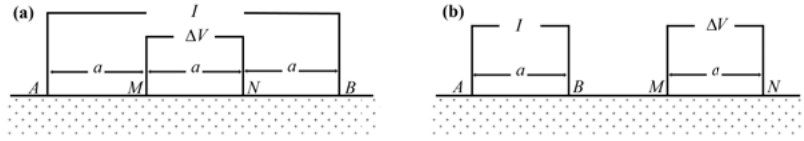

Figure 2.4. Sketch showing two typical geoelectric survey array types: (a) Wenner array and (b) Dipole-dipole array. Currents are injected through electrodes *A* and *B*. The voltage is observed through electrodes *M* and *N*. Spacing *a* represents distance between adjacent electrodes.

In a homogeneous Earth, the upper section of the earth above the depth of investigation (Loke, 1999) has the same influence on the measurements as the lower section. This depth determines roughly how deep the array type can resolve the subsurface structures (Loke, 1999).

2.5 Traveltime tomography

Seismic tomography is used to model subsurface velocities using seismic waves generated by a controlled source, such as weight-drop and explosives, or passive sources (natural earthquakes). It resolves the spatial distribution of seismic velocity or slowness (Iyer and Hirahara, 1993). P-, S-, and surface waves are usually used to recover slowness or velocity models. Different resolutions are obtained depending on the nature of the seismic sources and seismic receiver coverage (Nolet, 1987).

Ray tracing is used to determine the refraction wave paths by travel time (Fig. 2.5). The travel time of a seismic wave is a nonlinear function of the source and receiver locations. It refers the source and receiver spatial positions, original shot time, and velocity structure along the wave path (Benz et al., 1996). This nonlinear function can be written as Eikonal equation:

$$\left(\nabla t\right)^2 = u^2 , \tag{2.25}$$

or

$$t = \tau + \int_{l(u)} u\left(\mathbf{r}\right) dl , \tag{2.26}$$

where t is the traveltime, $u(\mathbf{r})$ is the slowness (inverse of velocity) of subsurface, τ is original shot time, and dl is the differential length along the ray path $l(u)$.

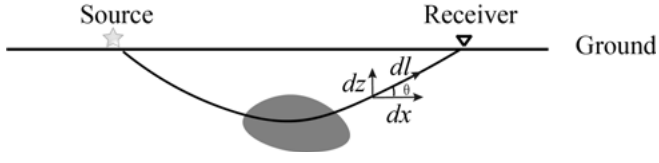

Figure 2.5. Sketch showing a ray generated by a source at the surface that passes through an anomaly and continues to receiver.

The ray travel path and travel time shown in Fig. 2.5 can be described as:

$$\frac{dx}{dt} = \frac{\cos(\theta)}{u}; \tag{2.27a}$$

$$\frac{dz}{dt} = \frac{\sin(\theta)}{u}; \tag{2.27b}$$

$$\frac{d\theta}{dt} = \frac{\partial c}{\partial x}\sin\theta - \frac{\partial c}{\partial z}\cos\theta. \tag{2.27c}$$

Equation 2.27a-c determines ray trace through inhomogeneous acoustic media. Ray tracing is an infinite-frequency approximation, and is valid if the seismic wavelength is small compared with size of the material anomaly (Eaton, 1999; Everett, 2013). To solve the Eikonal equation in 2D and 3D, the FDM is mostly used (Podvin and Lecomte, 1991; Pratt, 1999).

3 Theory of inverse problem

3.1 Occam inversion

In an inverse problem, an objective function of the form (Constable et al., 1987; Menke, 1989):

$$\begin{aligned}\Phi(\mathbf{m},\ \lambda) = &\left(\mathbf{d}-\mathbf{F}[\mathbf{m}]\right)^T \mathbf{W}_d^T \mathbf{W}_d \left(\mathbf{d}-\mathbf{F}[\mathbf{m}]\right) \\ &-Q_d^* + \lambda\left(\mathbf{m}-\mathbf{m}^r\right)^T \mathbf{W}_m^T \mathbf{W}_m \left(\mathbf{m}-\mathbf{m}^r\right)\end{aligned}, \tag{3.1}$$

is typically minimized with regards to the set of the model parameters $\mathbf{m} = \left(m_1,\ldots,\ m_M\right)^T$. The data vector $\mathbf{d} = \left(d_1,\ldots,\ d_N\right)^T$ contains N field data, and the vector $\mathbf{F}[\mathbf{m}]$ contains forward responses computed for a given model $\mathbf{m}$. The superscript T denotes matrix transposition. $\mathbf{W}_d = \text{diag}\left(\sigma_1^{-1},\ldots,\ \sigma_N^{-1}\right)^T$ is a data weighting matrix, where σ_i are the standard deviations of the observed data. $\mathbf{W}_m = \alpha_y\partial_y + \alpha_z\partial_z$ is the evolved model regularization term (Tikhonov et al., 1977; Constable et al., 1987), which guarantees the simplicity of the inverse model $\mathbf{m}$. The name of Occam inversion is given based on this simplicity (Constable et al., 1987; deGroot-Hedlin and Constable, 1990) and is widely known for inversion regularization. Vertical and horizontal smoothness operators ∂_y and ∂_z are shown in equations 3.2-3.3 when numbering the grid elements from top to bottom starting at the top left element. Both ∂_y and ∂_z are used when the near-surface structure is 2D (the targets are mainly in 2D in this thesis),

$$\partial_y = \begin{pmatrix} -1 & 0 & \cdots & 1 & & & & & \\ & -1 & 0 & \cdots & 1 & & & & \\ & & \ddots & & & \ddots & & & \\ & & & \mathbf{0} & & & & & \\ & & & & \ddots & & & \ddots & \\ & & & & & -1 & 0 & \cdots & 1 \\ & & & & & & \mathbf{0} & & \end{pmatrix}, \tag{3.2}$$

$$\partial_z = \begin{pmatrix} -1 & 1 & & & & & \\ & -1 & -1 & & & & \\ & & \ddots & \ddots & & & \\ & & & \mathbf{0} & & & \\ & & & & \ddots & \ddots & \\ & & & & & -1 & 1 \\ & & & & & & \mathbf{0} \end{pmatrix}. \tag{3.3}$$

$\mathbf{m}^r$ in equation 3.1 represents a reference model, which is constructed from an *a priori* information. The Lagrange multiplier λ balances data fit and model simplicity. Q_d^* represents the desired data misfit.

In individual inversion, Q_d and root mean square (RMS) error are defined as follows (Kalscheuer et al., 2013; Key, 2016):

$$Q_d\left[\mathbf{m}\right] = \sum\nolimits_{i=1}^{N_d} \left(\frac{d_i - F_i\left[\mathbf{m}\right]}{\sigma_i} \right)^2, \tag{3.4}$$

and

$$RMS = \sqrt{\frac{Q_d\left[\mathbf{m}\right]}{N_d}}, \tag{3.5}$$

where w_i is the data weighting factor.

By linearizing the forward operator in the vicinity of the current model $\mathbf{m}_k$, the minimization of the function $\Phi\left(\mathbf{m},\ \lambda\right)$ is simplified to minimizing the function $\Phi^{quad}\left(\mathbf{m},\ \lambda\right)$, which is quadratic in $\mathbf{m}_{k+1}$ (Menke, 1989),

$$\begin{aligned} \Phi^{quad}\left(\mathbf{m}_{k+1},\ \lambda\right) = &\left(\mathbf{d} - \mathbf{F}\left[\mathbf{m}_k\right] - \mathbf{J}\left(\mathbf{m}_{k+1} - \mathbf{m}_k\right)\right)^T \cdot \\ &\mathbf{W}_d^T \mathbf{W}_d \left(\mathbf{d} - \mathbf{F}\left[\mathbf{m}_k\right] - \mathbf{J}\left(\mathbf{m}_{k+1} - \mathbf{m}_k\right)\right) \\ &- Q_d^* + \lambda \left(\mathbf{m}_{k+1} - \mathbf{m}^r\right)^T \mathbf{W}_m^T \mathbf{W}_m \left(\mathbf{m}_{k+1} - \mathbf{m}^r\right) \end{aligned}, \tag{3.6}$$

where $\boldsymbol{J} = \left\{ \frac{\partial F_i\left[\mathbf{m}_k\right]}{\partial m_j} \right\}_{m=m_k}$ is the Jacobian matrix with elements of N rows and M columns. In the end, Occam approach can be used to solve the linearized equation 3.6 (deGroot-Hedlin and Constable, 1990; Rodi and Mackie, 2001; Kalscheuer et al., 2008; Key, 2016).

In addition to RMS, model resolution is another valid tool to evaluate inversion results. Model error and resolution analysis can be used to study model stability and closeness of an estimated model to the true one. The

ideal model resolution matrix is an identity matrix of size $M \times M$, which declares all model parameters are perfectly resolved (Menke, 1989). Generally, the estimated model parameters are weighted averages of the true ones (Kalscheuer et al., 2010). Thus, the row of the model resolution matrix that pertains to a certain investigation cell has non-zero entries also off its diagonal entry (referred to as spread; Menke, 1989). Typically the entries of a row of the model resolution matrix are scaled by the respective cell dimensions yielding a so-called resolving kernel.

3.2 Inverse theory of traveltime tomography

By linearizing equation 2.26 based on a starting slowness or velocity model, a system of equations can be derived as (Tryggvason et al., 2002)

$$\gamma_i^{P,S} = \mathbf{B}_i^P \Delta u^P + \mathbf{B}_i^S \Delta u^S + k\mathbf{L}_i^{P,S} + l\mathbf{S}_i \,, \tag{3.8}$$

where, γ_i is the vector of traveltime residuals, $\mathbf{B}_\mathrm{i}$, called the derivative kernel, is the matrix of distances travelled by a ray in each cell, Δu is the vector of slowness perturbations, $\mathbf{L}_i$ is the smoothness constraint for model parameters, and $\mathbf{S}_i$ controls the degree of V_p/V_s variation. P and S present P-wave and S-wave, respectively. k and l are regularization parameters that can be selected and tuned using a trade-off curve or cross-validation. The dataset used in this thesis, however, only provides first arrivals of P-waves, since S-waves are difficult to distinguish in the shot gathers. LSQR (Paige and Saunders, 1982), an efficient and accurate conjugate gradient solver, is used to solve equation 3.8. The first arrivals are modelled based on a finite-difference solution for the Eikonal equation 2.26 (Podvin and Lecomte, 1991).

3.3 Joint inversion of boat-towed RMT and lake-floor ERT data

Joint inversion of boat-towed RMT and lake-floor ERT has the possibility of improved structural imaging for near-surface applications, providing better resolution than any individual inversion due to improved data coverage, complementation of data sensitivity to model, and better suppressed data noises.

In order to implement this type of inversion, the original inversion code EMILIA was modified (Kalscheuer et al., 2008, 2010). 2D forward modelling of both RMT and ERT data in the code is handled with FDM (Dey and Morrison, 1979; Siripunvaraporn and Egbert, 2000; Kalscheuer et al., 2008). The forward responses and sensitivities of ERT in EMILIA have been modified to be suitable for potential fields generated by electrodes at arbitrary

positions. Another wavenumber selection for Fourier transformation along the strike direction and inverse Fourier transformation is added in EMILIA (Xiong and Wang, 2011). $\mathbf{F}[\mathbf{m}_k]$ has also been changed to represent either resistances or apparent resistivities, due to the difficulty of using apparent resistivity meaningfully when electrodes are at arbitrary positions, for example, half at the water bottom and half at the ground surface. The inversion theory has been described in the section 3.1.

The differences of joint inversion and single inversion shown in equations 3.1-3.6 are given in following text. In joint inversion of boat-towed RMT and lake-bottom ERT data, the model vector **m** contains resistivity values. The data vector **d** contains apparent resistivity and phase values for RMT method, and resistance for ERT method. The vector $\mathbf{F}[\mathbf{m}]$ contains the same data type as **d**.

The following definition of a scaled and weighted misfit function $Q_{d,sw}$ is used for the joint inversion (Kalscheuer et al., 2013):

$$Q_{d,sw}[\mathbf{m}] = \frac{N_d}{\sum_{j=1}^{N_{ds}} \sum_{i=1}^{N_j} \left(\frac{1}{w_{ji}} \right)^2} \sum_{j=1}^{N_{ds}} \sum_{i=1}^{N_j} \left(\frac{1}{w_{ji}} \frac{d_{ji} - F_{ji}[\mathbf{m}]}{\sigma_{ji}} \right)^2 , \quad (3.8)$$

where N_d is the number of all data points, N_{ds} is the number of datasets, N_j is the total number of data points in dataset j, w_{ji} is dataset weighting factor, and σ_{ji} is the standard deviation of d_{ji}. The RMS calculation method, however, is the same as equation 3.5.

3.4 Joint inversion of boat-towed RMT and boat-towed CSMT data

Joint inversion of boat-towed RMT and CSMT data has the possibility of improved structural imaging for near-surface applications (Key, 2016). In order to implement this type of inversion, the original inversion code MARE2DEM was modified to handle the CSRMT data collected by the instrument Enviro-MT. The 2D forward modelling part of the code is handled with FEM (Li and Key, 2007; Key and Ovall, 2011). The forward responses and sensitivities of controlled source electromagnetics (CSEM) in MARE2DEM have been modified to be suitable for an impedance tensor. Wavenumbers are quantitatively increased for the inverse Fourier transformation along the strike direction to model high-frequency CSMT data. $\mathbf{F}[\mathbf{m}_k]$ represents logarithmic impedance due to the fast convergence of using this type of input in the inversion. The general procedure of inversion is also covered in section 3.1.

In joint inversion of boat-towed RMT and CSMT data, the model vector **m** is resistivity values, the data vector **d** contains apparent resistivity and phase values for RMT method and impedance data for CSMT method, and the vector $\mathbf{F}[\mathbf{m}]$ contains the same data type as **d**.

To alleviate the dominance of one dataset in the joint inversion, a normalized joint misfit is implemented as (Key, 2016):

$$\begin{aligned}&\alpha_1\left(\mathbf{d}_1-\mathbf{F}_1[\mathbf{m}]\right)^T\mathbf{W}_{d1}^T\mathbf{W}_{d1}\left(\mathbf{d}_1-\mathbf{F}_1[\mathbf{m}]\right)+\\&\alpha_2\left(\mathbf{d}_2-\mathbf{F}_2[\mathbf{m}]\right)^T\mathbf{W}_{d2}^T\mathbf{W}_{d2}\left(\mathbf{d}_2-\mathbf{F}_2[\mathbf{m}]\right)=\frac{\chi_1^2}{n_1}+\frac{\chi_2^2}{n_2}\end{aligned}\quad , \tag{3.9}$$

where

$$\alpha_i=\sqrt{1/n_i} \tag{3.10}$$

is a data weighting that balances data misfit so that a smaller dataset will have as much influence as a larger subset on the overall misfit. Additionally, this parameter can be adjusted manually, increasing or decreasing the weight on data regardless of size. n_i is the number of data points in each dataset. χ_i is the desired data misfit for each dataset. A model then fits both datasets satisfying

$$\frac{\chi_1^2}{n_1}+\frac{\chi_2^2}{n_2}\approx 1+1\,. \tag{3.11}$$

4 Summary of papers

4.1 Paper I: Geophysical characterization of areas prone to quick-clay landslides using radio-magnetotelluric and seismic methods

In this paper, high-resolution seismic and RMT data were used together to map potential quick clays and related potential landslide areas near the Göta River in southwest Sweden. If subsurface distribution of quick clays and their host structures are better understood, influences, such as financial losses, damages in transportation systems, and fatal causalities, caused by quick-clay landslides can greatly be mitigated. Because the resistivity and velocity of quick clays and their underling coarse-grained layer are different compared with their surrounding marine clays, RMT and seismic tomography were chosen in this study to delineate quick clays and to understand their host materials. Velocity and resistivity models constrained from first-arrival traveltime and RMT data were used to delineate quick-clay distribution, subsurface geology, and coarse-grained materials. The resistivity and tomographic velocity models suggest a much larger role of the coarse-grained materials at the site than previously thought, which may also act as a slip surface for landslides. The erosion of the riverbank when close to the river and human activities when away from the river are the two main scenarios for quick-clay landslides to occur under special geological conditions. These two possibilities were derived in this study with the help of RMT and first-arrival traveltime tomography.

4.1.1 Quick clays

Quick clay is defined as a clay with remolded shear strength less than 0.4 and 0.5 kN/m^2 (by fall cone test) and sensitivity larger than 50 and 30 (high sensitivity) in Sweden and Norway, respectively (Rankka et al., 2004; Donohue et al., 2012; Wang et al., 2016). The sensitivity is defined as the ratio between undrained, undisturbed shear strength and the remolded shear strength (Solberg, 2007; Shan et al., 2014; Wang et al., 2016). Undisturbed quick clay resembles a water-saturated gel that has formed through flocculation and deposition (Rankka et al., 2004) during and after the last glacial period (> 10-12 kyr). Undisturbed shear strength of quick clay has the same in-situ mechanical behavior as non-quick clay.

Due to the isostatic land uplift during the last de-glaciation period, marine clays have been subjected to rise up and through time exposed more and more to infiltrated fresh water (Brand an Brenner, 1981). Thus, salt in the pores of marine clays have been infiltrated out by fresh/rain water from surface or through bedrock surface (Malehmir et al., 2013a, 2013b; Shan et al., 2014). Higher electrical resistivity is presented in leached clay due to the reduction in the salt content and the structures change of the clay. Quick clays can be liquefied due to a sudden change in stress, for example caused by uploading or unloading pressure, and because of their high sensitivity. Stress change as small as the touch of a human hand can liquefy a lab sample of quick clay (Malehmir et al., 2013b). For large deposits, greater stress changes, such as increased saturation by rainwater, are required (Malehmir et al., 2013b).

4.1.2 Study area and available data

The study area is located near the Göta River (Fig. 4.1), north of the municipality of Lilla Edet in southwest of Sweden. Along Göta River several

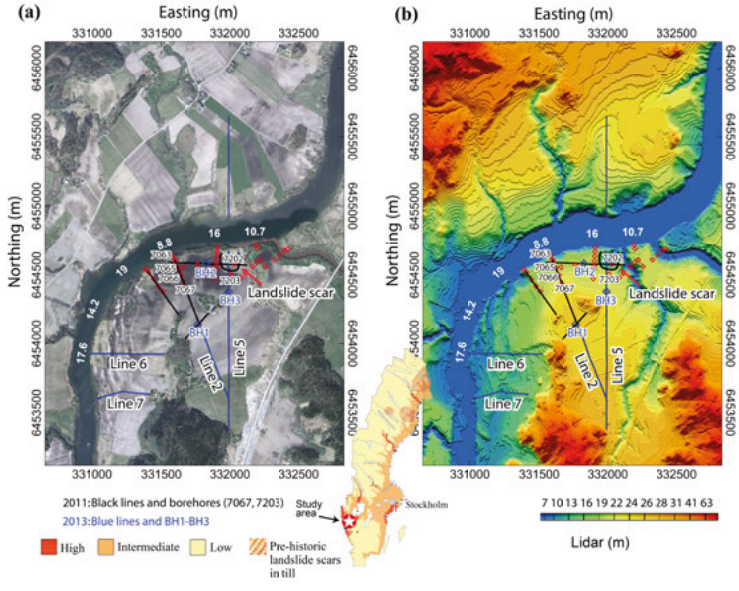

Figure 4.1. (a) Airphoto and (b) LiDAR map showing the locations of the geophysical lines in the study area (from Wang et al., 2016). Black and blue lines were surveyed in 2011 and 2013, respectively. A landslide scar is marked by black curve. Blue circles represent boreholes drilled in 2013. Red circles are geotechnical boreholes from the Swedish Geotechnical Institute (SGI). Water depth is marked by white numbers.

catastrophic landslides have occurred (e.g., Lilla Edet 1957; AB Svensk Filmindustri, 1957). Post-glacial tills are the dominant materials in the

southern margin of the river. Based on the LiDAR (light detection and ranging) elevation data (Fig. 4.1), highland areas are highly occupied with shallow or exposed crystalline bedrock of granite-gneiss and granodiorite. Silty and coarse-grained materials are often found within clayey materials (Salas-Romero et al., 2016). A quick-clay landslide scar, 30-40 years old, with a retrogressive shape is observed in the study area (Fig. 4.1). The base of the landslide consists of coarse-grained materials (speculated by Malehmir et al., 2013a), implying that the coarse-grained materials may play a key role in controlling the scale of any potential landslide at the site. From three cored boreholes in the sediments (BH1-BH3, Fig. 4.1, Salas-Romero et al., 2016), coarse-grained materials (of various thickness, around 10-30 m) underlying quick clays were observed. Bedrock was at about 80 m depth close to the river and at shallower depths towards the south.

This study was conducted as the continuation of a SEG-GWB (SEG, 2017) sponsored project studying quick-clay landslides in Nordic countries. A number of geophysical methods namely ERT, RMT, ground penetrating radar (GPR), gravity and magnetics as well as P- and S-wave refraction and reflection seismics have been used in this study area (Krawczyk et al., 2013; Malehmir et al., 2013a, 2013b, 2016; Shan et al., 2014, 2016; Salas-Romero et al., 2016; Wang et al., 2016). Four new geophysical profiles were designed in 2013 to complement those of 2011 but focusing this time on seismic and RMT methods; lines 2 and 5 were extended and lines 6 and 7 were newly acquired (Fig. 4.1).

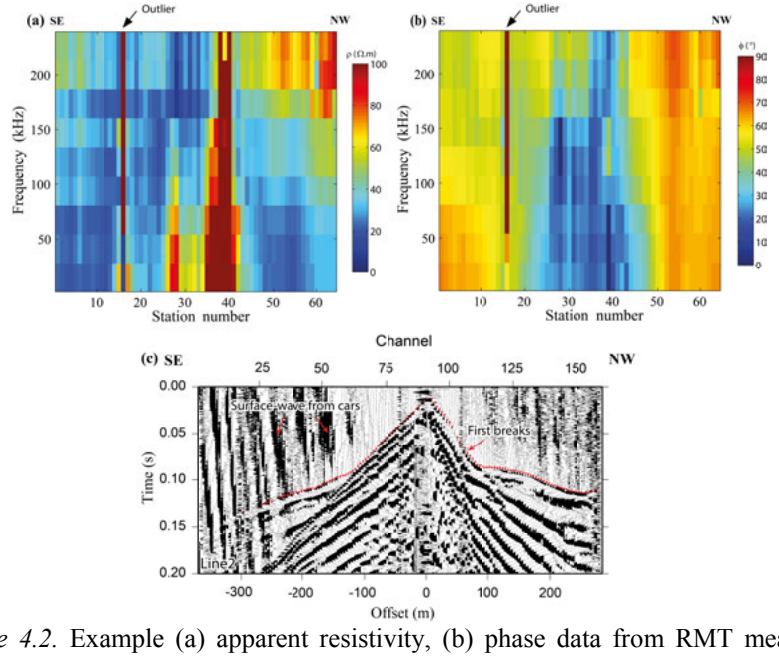

Figure 4.2. Example (a) apparent resistivity, (b) phase data from RMT measurements, and (c) raw shot gather along line 2 showing data quality. A few outliers were excluded from the inversion.

Table 4.1 summarizes the main parameters used for the RMT data acquisition in this study. EnviroMT system (Bastani, 2001) was used for data acquisition. An example of raw apparent resistivity and phase data from line 2 is shown in Fig. 4.2a,b.

Table 4.1. *Main RMT data acquisition parameters, 2013 (Wang et al., 2016).*

Survey parameters	Line 2	Line 5S[1]	Line 5N[2]	Line 7
Recording system	EnviroMT	EnviroMT	EnviroMT	EnviroMT
No. of stations	43	128	31	48
No. of transmitters	> 20	> 20	> 20	> 20
Station interval (m)	10	10	10	10

1: Line 5 southern side of the river; 2: Line 5 northern side of the river.

Table 4.2. *Main seismic data acquisition parameters were used in the 2013 survey. The 2011 seismic data acquisition parameters can be found in Malehmir et al. (2013b) and Wang et al. (2016).*

Survey parameters	Line 2	Line 5	Line 6	Line 7
Recording system	SERCEL 428	SERCEL 428	SERCEL 428	SERCEL 428
No. of receivers	160	398	133	100
No. of shots	157	87	130	100
Receiver interval (m)	4	4/10	4	4
Shot interval (m)	4	20	4	4
Maximum offset (m)	640	2247	528	396
Source type	WD[1]	Ex[2]	WD[1] / H[3]	H[3]
Charge size (gr)		50-200		
Record length (s)	6	10	10	10
Sampling rate (ms)	0.5	0.5	0.5	0.5
Geophone frequency (Hz)	28	28/10/MEMs	28	28
No. of geophones per set	Single	Single	Single	Single
No. of shots/point	5	1	5	3-5
Shot depth (m)	0	0.5-1	0	0

1: Weight-drop; 2: Explosive; 3: Sledgehammer.

Table 2 summarizes the main parameters for the seismic data acquisition. A Sercel 428 recording system was used for the data acquisition. Single-component wireless recorders were also used to cover the northern part of the study area on the other side of the river (e.g., Malehmir et al., 2015; Brodic et al., 2015). Fig. 4.2c shows example shot gathers from line 2. First arrivals are clearly shown on all these lines and particularly noticeable on the longest line.

4.1.3 Results and interpretations

Only the results from the inversions and comparisons between the geophysical and geotechnical data of line 2 are shown here and in the following text (Fig. 4.3). The same distance along the lines to define the location of various data is used for consistency purposes.

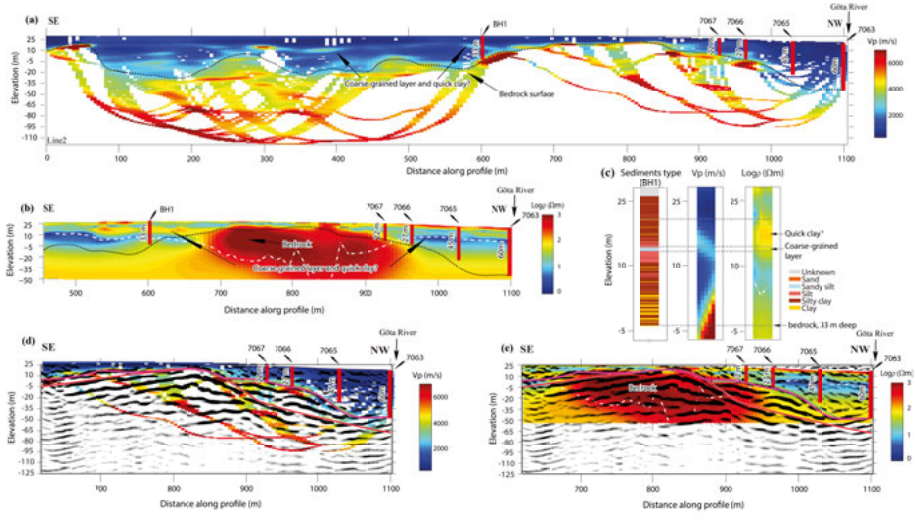

Figure 4.3. (a) Tomography and (b) RMT models of line 2. (c) Correlation between borehole data (BH1) and the models close to the borehole. (d) and (e) showing available reflection seismic data (from 2011) superimposed on the velocity and resistivity models, respectively. Same depth and distance scales are used in all the subfigures for comparison. RMS (root mean squared difference between observed data and modelling responses) of resistivity model is 1.8 and RMS (root mean squared time residual) of tomography is 2.2 ms. Geotechnical boreholes 7066 and 7067 show good correlation with the reflection, resistivity and tomography results. Black dashed lines in (a) and (b) and violet lines in (d) and (e) represent bedrock surface obtained from tomography. The white dashed line in (b) and (e) represents penetration depth of the RMT data. Solid red and green lines in (d) and (e) represent the structure boundaries in bedrock obtained from reflection.

Line 2 is the second longest in the study area and ends close to the bank of the Göta River (Fig. 4.1). Borehole BH1 is at about 600 m distance along the

line. The bedrock depth of approximately 10 m north of BH1 (Fig. 4.3a,b), high velocity and resistivity boundaries, was suggested by both RMT and seismic tomography models. Bedrock depressions indicating the possibility of landslide are quite visible in the tomography results (Fig. 4.3a). A layer of higher velocity (around 1700-2500 m/s) is observed in the tomography results, which corresponds well to the coarse-grained materials in BH1 (Fig. 4.3a). In the RMT model, this layer appears as a resistive layer (Fig. 4.3b) suggesting that there may be quick-clay and fresh-water-saturated coarse-grained materials. Fig. 4.3c illustrates the comparison between the models and borehole information (Salas-Romero et al., 2016). The bedrock surface is also well resolved.

The first-arrival traveltime tomography and RMT models were superimposed on reflection seismic section of a portion of the line from 2011 for comparisons (Fig. 4.3d,e). Generally, there is a good match among the RMT, tomography, seismic reflection, and available geotechnical boreholes, altogether verifying these results.

4.1.4 Discussion and conclusions

The resistivity of quick clay varies normally from 10 to 100 ohm-m (Solberg et al., 2012; Long et al., 2012; Karlscheuer et al., 2013; Shan et al., 2014, 2016; Wang et al., 2016). Compared with the surrounding marine clays (< 10 ohm-m), quick clays show higher resistivities. They are often found right above the coarse-grained materials in this study area (Malehmir et al., 2013a, 2013b, 2016; Salas-Romero et al., 2016; Wang et al., 2016), and strong seismic reflection and tomographic characterization are resolved for the combination of quick clays and underlying coarse-grained materials (Fig. 4.3a).

Combining all the features discussed above, sedimentary units consisting of both quick clays and coarse-grained materials together show relatively high velocity and high resistivity features when compared with their surrounding marine clays. All those characterized areas along our survey lines are near to the riverbank, which is usually one of the most suitable places for easily triggering quick-clay landslides (Nadim et al., 2008).

Synthetic tests show that the RMT data are likely unable to distinguish between quick-clays and coarse-grained materials if they are juxtaposed and sandwich each other, and surrounded by the low-resistivity marine clays. This indicates resistivity measurements should be supplemented by geotechnical investigations as suggested by Andersson-Sköld et al. (2005).

Triggering quick-clay landslides is determined by topography, erosion potential, and geotechnical properties. The new geophysical lines provide a better understanding of the geological features at the research site, resolve bedrock at different parts, and help to display the development of quick-clay landslide at the research site. The conclusion is that the mini-basin shape of bedrock suggests the possibility for generating quick-clay landslide only

likely if the toe of the materials is removed (like road constructions, region A in Fig. 4.4). When the area is close to the river, erosion at the riverbank could play an important role (region B in Fig. 4.4). Potential quick clays resolved in the models at the southern side of the river imply that this region may be susceptible to quick-clay landslides in the near future.

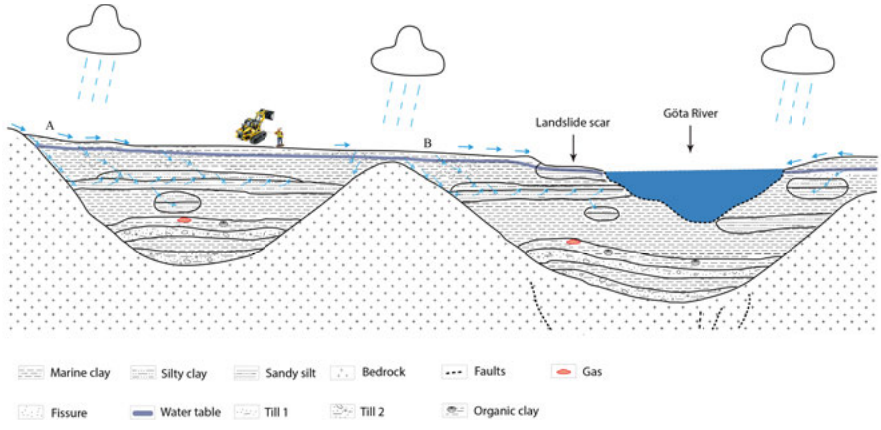

Figure 4.4. Sketch showing potential roles of the bedrock and coarse-grained materials in the deformation of quick clays and plausible landslide triggering mechanisms. For the bowl-shaped bedrock (region A), landslide triggering would require removal of sediments like construction work; for the erosion part along the river (region B), accumulated or sudden change in pore pressure in the quick clays is necessary to trigger landslides. In both scenarios, coarse-grained materials and bedrock surface would contribute to the formation of quick clays and the process of an eventual landslide.

RMT and seismic methods have successfully been used to extend earlier studies on delineating quick-clay zone and subsurface geology of an area prone to landslide in southwest Sweden. Four lines were surveyed for these reasons (see Wang et al., 2016). Both electrical resistivity and seismic velocity models have in many places good accordance with the existing borehole observations and reflection seismic sections. The data in particular can resolve the bedrock undulation, and more importantly an extended coarse-grained layer overlapping the bedrock is identified in most models. The shape of the bedrock and the location of quick clays and coarse-grained materials determine two different mechanisms for triggering quick-clay landslides at the site. Future studies are required to validate these interpretations and joint inversion of RMT and traveltime tomography is recommended for better delineation of quick clays and bedrock surface.

4.2 Paper II: Joint inversion of lake-floor electrical resistivity tomography and boat-towed radio-magnetotelluric data illustrated on synthetic data and an example application from the Äspö Hard Rock Laboratory site, Sweden

The ERT method provides moderately good constraints for both conductive and resistive structures while the RMT method is well suited to constrain conductive structures. Additionally, RMT and ERT data may have different target coverage and are differently affected by various types of noise. Thus, joint inversion of RMT and ERT datasets may better constrain the resultant model compared with single inversion. In this paper, joint inversion of boat-towed RMT and lake-floor ERT data was for the first time formulated and implemented. A synthetic test together with a case study from an area adjacent to the Äspö HRL in south-eastern Sweden was used to illustrate the implementation of the joint inversion approach. A 790-m-long profile comprising lake-floor ERT, boat-towed RMT data, and partial land RMT data was used in the field application. Joint inversions were performed with or without weighting (applied to different datasets, vertical and horizontal model smoothness), along with the constraints of bathymetry and water resistivity measurements, and compared. The results show that a major north-easterly oriented fracture system, NE-1, observed in the HRL facility and boreholes together with a previously uncertain weak zone, EW-5, are delineated in this study.

4.2.1 Synthetic example for single and joint inversions

In order to handle the joint inversion of boat-towed RMT and lake-floor ERT data, modification of the code EMILIA (Kalscheuer et al., 2008) was needed. The ERT modelling part was modified to suit for electrodes located at arbitrary positions. Comparison between EMILIA and RES2DMOD (Loke, 2002) was done to verify the modification. It was observed that the relative differences ($(\rho_{res} - \rho_{emilia})/\rho_{res} \times 100\%$) of forward modelling for same parameterization between these two codes were less than 1.8%. Afterwards, a synthetic example was represented. The synthetic model (Fig. 4.5a) was constructed from single inversion of ERT field data. Most important features in the model are a fracture zone (100 ohm-m) extending from 600 to 650 m along the profile and dipping with an angle of about 50°. EMILIA was used to calculate the RMT responses on the surface including water and land data and the ERT responses on land and at the bottom of the water body. The Gaussian noises with 5 % on ERT resistance, 10 % on RMT apparent resistivity and 2.29 degrees on RMT phase data were added in the synthetic data to keep the noise level comparable to the field data.

The differences between individual and joint inversions with the synthetic datasets were compared with details. Here only the joint inversion of RMT TE-mode and ERT data is selected to show (details can be found in **Paper II**). For the RMT TE-mode and ERT data, the current flows are parallel and predominantly perpendicular to the plane of the profile, respectively. Thus, their joint inversion leads to more complementary model constraints than joint inversion of RMT TM-mode and ERT data (details can be found in the appendix of **Paper II**).

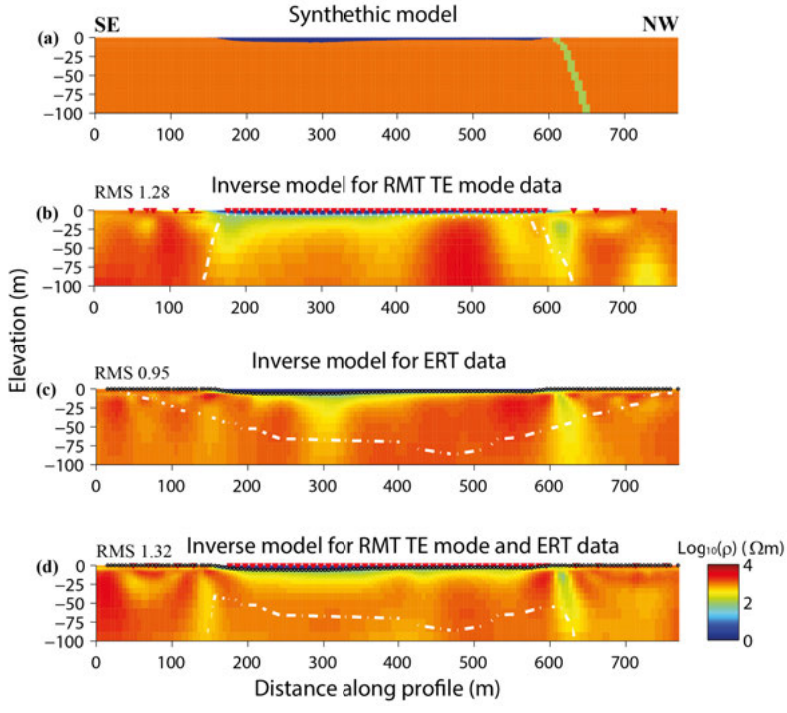

Figure 4.5. (a) Synthetic model. (b) Individual inversion model of RMT TE-mode data. (c) Individual inversion model of ERT data. (d) Joint inversion model for RMT TE-mode and ERT data. Total RMS is 1.32 (RMS of RMT data is 1.32, RMS of ERT data is 1.32). Black dashed line shows the approximate exploration depth of the signals used in the inversion. In the models, RMT and ERT stations are marked by red triangles and white dots, respectively.

The individual inversion model for the RMT TE-mode data shows that the fracture zone is not well resolved (Fig. 4.5b). The individual inversion of ERT data shows a similar result (Fig. 4.5c). Black dashed lines represent the maximal exploration depths of the RMT and ERT datasets in the models estimated using Spies' (1989) method and Dahlin and Zhou's (2006) method as discussed in Section 2.1 and 2.4, respectively. The RMT exploration depth was calculated using 14 kHz frequency and the vertical resistivity section in the model. The joint inversion of RMT TE-mode and ERT data

generated a model very similar to the true model (Fig. 4.5a,d). It is particularly demonstrated with the dipping angle of the fracture zone. Besides, water body and fracture zones are more accurately resolved in the joint inversion than in any individual inversions.

4.2.2 Geology and field data

The case study area, Äspö, is located near the shoreline of the Baltic Sea in south-eastern Sweden (Fig. 4.6a). Granitic rocks dominate the site and diverse types of fractures or fracture zones are both geologically and geophysically inferred (Cosma et al., 2001). Most fracture zones at Äspö are a result of reactivation of older structures and appear mainly brittle. The Baltic Sea is connected to the measurement area through a narrow water channel. The Äspö HRL, operated by the Swedish Nuclear Fuel and Waste Management Company (SKB), is located at the northern side of the measurement area. Approximately 500 m southwards from the measurement area, a nuclear power plant is located. A tunnel plunging at about 14% over a length of about 1500 m connects the surface to the HRL (450 m deep) as well as various smaller tunnels, ramps and one main shaft (Almén and Stenberg, 2005). During tunnel excavation, a NE-SW running fracture system (known as

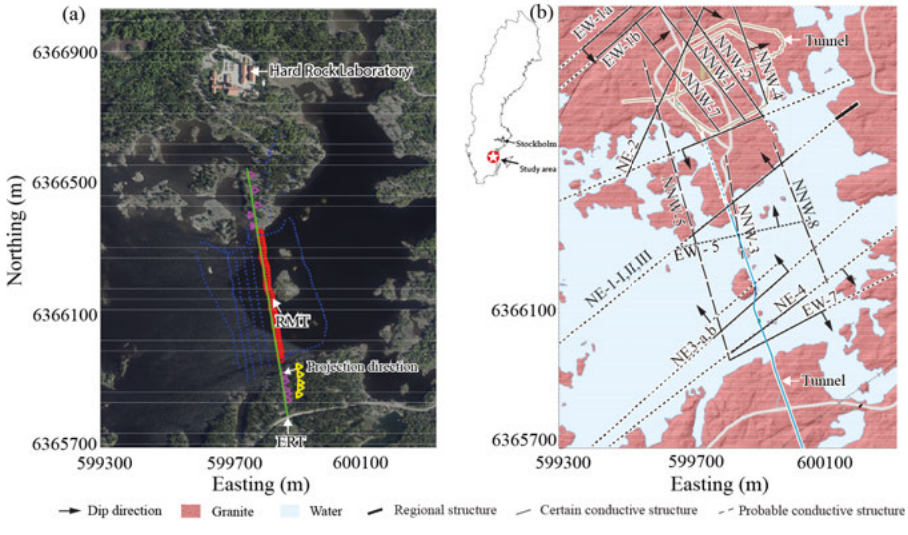

Figure 4.6. (a) Aerial photo (Image © Google) and (b) geological map of the case study area (courtesy of Geological Survey of Sweden (SGU)). RMT profiles are marked by different symbols with different colors. The RMT profile used for the joint inversion is marked by red circles on the lake and pink triangles on the land. ERT data were measured only along one profile, marked by green dots. Positions of fracture zones, which are documented by SKB, are shown in (b). However, their surface projections are based on limited tunnel and boreholes observations combined with low-resolution geophysical data. The general topography of the land part is approximately flat.

NE-1) was observed below the northern-end of the RMT lake profile (Fig. 4.6b). At approximately 1300 m along the tunnel, the NE-1 fracture system is intersected at approximately 180 m depth below ground surface (Almén and Stenberg, 2005). Three main subsets comprise the NE1 fracture system and that is about 60 m wide in total (Berglund et al., 2003; Rhén et al., 1997). The two southernmost subsets are described as highly fractured and hydraulically conductive (Stanfors et al., 1999; Makurat et al., 2006; Berglund et al., 2003). Using tunnel and cored borehole observations, the dipping of NE-1 fracture system is refereed as a 65 degree. Thus, uncertainty exists because information gaps between the tunnel and the boreholes are not effectively filled (Berglund et al., 2003). Three fracture zones namely EW-7, NE-4 and NE-3 on the southern part of the RMT profile below the lake (Fig. 4.6b) were indicated by refraction seismic (not public access) and borehole data (Wikberg et al., 1991; Stanfors et al., 1999; Rhén et al., 1997). Geological information suggests the existence of the fracture zone EW-5 (Fig. 4.6b) (Wikberg et al., 1991); this, however, is not confirmed in tunnel observations.

The Enviro-MT was used for RMT data acquisition (Bastani, 2001). On the lake the station spacing was around 10 m, while on land the spacing varied from 20 to 40 m depending on the ground conditions (Fig. 4.6a). In total 52 stations were surveyed. Compared with the land part, the boat-towed RMT data acquisition was extremely efficient. Within 2.5 hours, all the RMT stations on the lake were surveyed (Fig. 4.6a) in contrast with two days used to acquire the land data (Fig. 4.6a). RMT stations surveyed and used for joint inversion are marked by red circles and pink triangles.

The Terrameter LS instrument was used for ERT data acquisition with a multiple gradient array (Dahlin and Zhou, 2006). The ERT line was extended by roll-along technique based on 635 m long ERT electrode spread to a total length of 790 m. More details of the ERT data acquisition are shown in Ronczka et al. (2017). Green dots mark the ERT stations used for joint inversion in Fig. 4.6a.

The field datasets show an average quality (Wang et al., 2017a). The RMT TE-mode apparent resistivity and phase data at water part indicate that the seawater has slightly higher resistivity than the lake-bottom sediments. Due to the small thickness of water and sediments (< 3.5 m) along 50% the profile and around 20% of the RMT stations are on land, the RMT data can provide useful information in inversion for resistive bedrock and the lake sediments. Before inversion, strike analysis of RMT data has been done to guarantee the 2D assumption. Since the ERT cable was placed on the lake floor, the ERT penetration depth in the underlying resistive basement is not reduced strongly by the overlying conductive water. A 10% relative error floor was used for the RMT apparent resistivity data (30% relative error floor was used for the land stations), an absolute error floor of 2.29 degrees was used for RMT phase data, and a 5% relative error floor was used for the ERT data.

4.2.3 Inversion and evaluation

The inversion was done employing a two-step inversion strategy (Wang et al., 2017a). In the first step, an Occam inversion using regular smoothness (Constable et al., 1987; Menke, 1989) was used with Lagrange multiplier and a 100 ohm-m half space was used as initial model. In the second step, the best inversion model from step one was then used as a new initial model in an Occam inversion with additional Marquardt-Levenberg damping. The models from individual and joint inversions of the field data are shown in Fig. 4.7. Both individual inversions show common features, such as the water body and the island in the middle of profile (Fig. 4.7a,b). The fracture zones at 550-700 m distances along the profile are not well reconstructed. Besides, ERT model cannot fit RMT data and vice-versa. However, at the

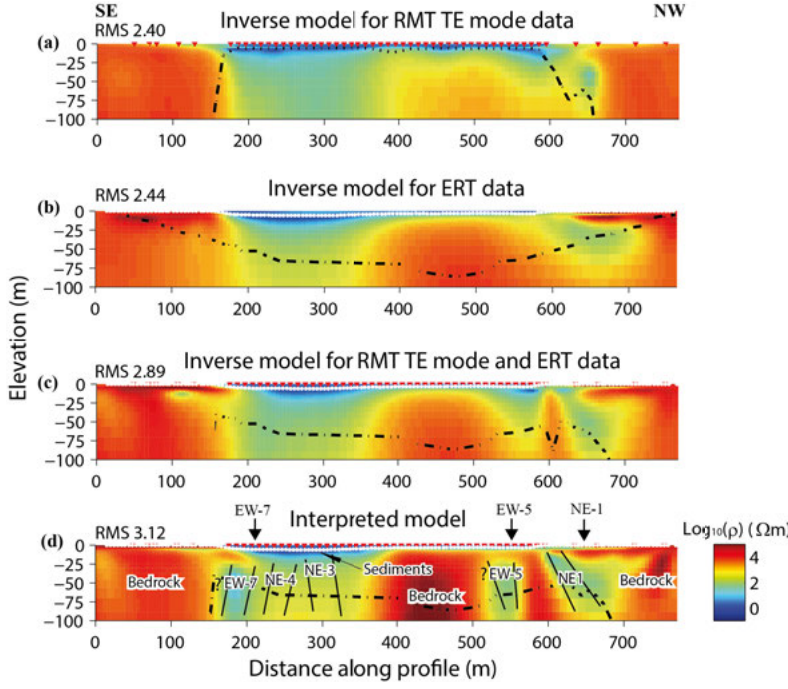

Figure 4.7. (a) Inversion model for RMT TE-mode data. (b) Inversion model for ERT data. (c) Joint inversion model for RMT TE-mode and ERT data. Total RMS is 2.89 (RMS of RMT is 3.36 and RMS of ERT is 2.69). (d) Joint inversion model constrained with bathymetrical data and water resistivity measurement. Total RMS is 3.12 (RMS of RMT is 4.28 and RMS of ERT is 2.56). Separate RMS values from joint inversion are slightly higher than those of the single inversions. However, the model fits both datasets with acceptable RMS.

550-700 m distance a strong similarity between the conductive structures in both models is shown (Fig. 4.7a,b). The joint inversion model (Fig. 4.7c) shows two relatively conductive zones at 550-700 m distance along the pro-

file. Compared with single inversions, the joint inversion model can fit two different geophysical datasets simultaneously.

Bathymetry data were also acquired during the boat-towed RMT measurement. The water resistivity was measured at three different water levels (Ronczka et al., 2017). Thus, an *a prior* model ($\boldsymbol{m}^r$ in equation (3.6)) was built on these information. The water resistivity measurements at three different depths (1.48 ohm-m at 0.2 m depth, 1.37 ohm-m at 3.8 m depth, and 1.28 ohm-m at 4.8 m depth.) can be used to fix the resistivity of the lake water in the inversion. The *a priori* model had two structures, the water body and the bedrock with a resistivity of 225 ohm-m. Three different types of water resistivity models are used: (1) homogeneous water, (2) three-layered water, and (3) multi-layer water with resistivity changing linearly based on the three measurements. Below the lake floor, more conductive sediments were observed in previous inversions. Hence, the decoupling of the smoothness constraint along the lake floor guarantees the free search of the model parameters across the lake floor. The *a priori* model is also used as initial model in step one.

The joint inversion model (without using any weight technique) of the RMT TE-mode and ERT data constrained by bathymetry and measurements of water resistivity (Fig. 4.7d) is similar to the results without these constraints. However, the shape of sediments is more focused in this model and bedrock resistivity is better resolved. Water model (2) was used after comparison. Three fracture zones, NE-1, EW-5, and EW-7 are visible in the model (Fig. 4.7d). Only the fracture zone NE-1 is well confirmed from tunnel and borehole observations. The fracture zones EW-5 and EW-7 need to be further verified. In the constrained joint inversion (Fig. 4.7d), a relatively large misfit is observed compared to normal joint inversion (Fig. 4.7c). This is related to the fact that the approximation of water with three layers is not accurate enough to represent the real spatial variation of water resistivity. However, the part below the water zone gives even better misfit in contrast with single inversions or other joint inversions without constraint with bathymetry data and water resistivity (Table 4.3 and Fig. 4.8). All these features together with model resolution analyses (shown in **Paper II**) indicate

Table 4.3. *Average RMT data differences for different types of inversions corresponding to Fig. 4.8 (for examples, type **a** and type **c** in the table correspond to Fig. 7a and 7c, respectively). The three highest frequencies mainly relating to saline water are excluded due to the insufficient measurement of water resistivity. The constrained joint inversion (type **d**) has better data differences than the single inversions.*

Inversion type	a	c	d
Average ρ difference	2.08	2.59	1.93
Average φ difference	0.79	1.16	1.24

the improved resolution of our new implementation in this complex environment compared with single inversion.

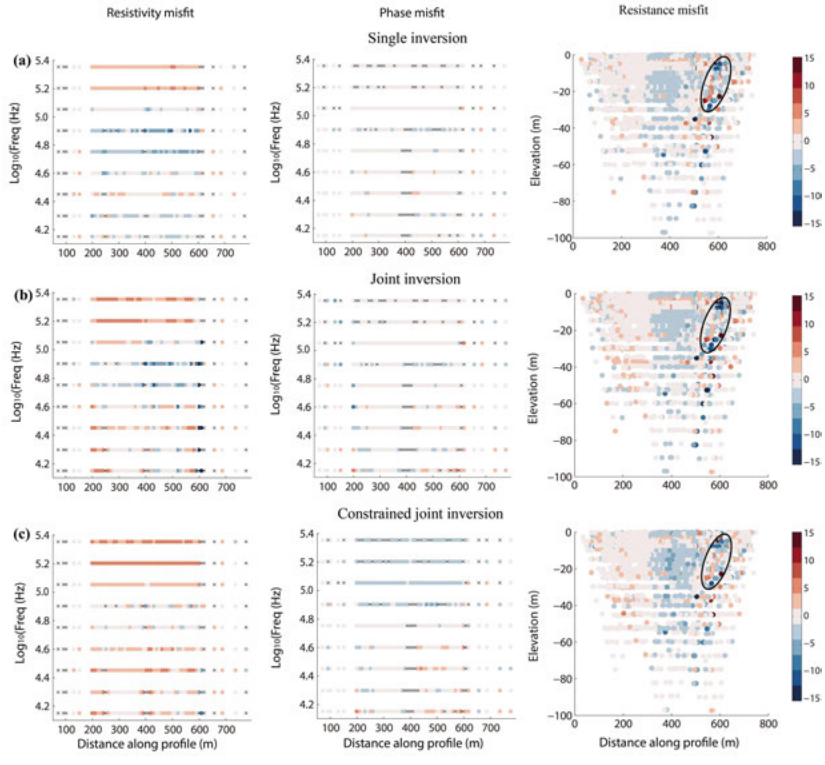

Figure 4.8. Data differences between field and inverse modelled RMT and ERT data from (a) RMT TE-mode and ERT data single inversions; (b) joint inversion without using any weighting and constraint; (c) constrained joint inversion model with bathymetrical data and water resistivity measurements. The constrained joint inversion with bathymetry data and water resistivity measurement has comparable or better RMS misfits compared with the single inversions.

4.2.4 Discussion and conclusions

The implementation of joint inversion of boat-towed RMT and lake-floor ERT data was tested with both synthetic and field datasets. All the results demonstrated that the joint inversion is better than any individual inversions. Three reasons can be mentioned for this: (1) the two datasets lead to improved data coverage of geological targets, (2) the sensitivities of the two methods complement each other (Candansayar and Tezkan, 2008; Kalscheuer et al., 2010), and (3) the two methods are affected differently by noise.

An *a priori* model provides known information to the inversion model, hence ambiguity can be partly reduced in those parts of the model. Uncertain model parameters, therefore, become better constrained. The water resistivities, obtained from direct measurements, were fixed in the constrained joint

inversion with decoupled smoothness along the water bottom. By doing so, the joint inversion improved the inversion results for imaging the fracture systems (Fig. 4.7).

Data misfit analyses, exploration depth investigations, and model resolution analyses (see in **Paper II**) were three methods to evaluate the inversion models when they have reasonable RMS. The well-constrained part in the models is distinguished by passing all three evaluation methods. Only in this way, the well-constrained part of the model is representative of the subsurface structures. Three fracture zones are detected in the constrained model (Fig. 4.7d). However, NE-1 is well resolved, EW-5 is partly resolved and needs to be further verified, and EW-7 is poorly resolved. A synthetic test based on the interpretation showed the datasets behaviour (Wang et al., 2017a). The results show that using boat-towed RMT and lake-floor ERT together would have higher resolution, if the water and sediments had been less conductive. This method can effectively resolve underwater structures and reduce the cost of pre-investigations for under-water infrastructure planning projects.

4.3 Paper III: Using boat-towed controlled source radio-magnetotelluric data to resolve fracture zones at the Äspö Hard Rock Laboratory site, Sweden

As a continuation of the previous study (**Paper II**), the boat-towed controlled source RMT method was implemented and used to resolve the fracture zones. The boat-towed RMT system is attractive to be used on shallow water regions. However, the lowest frequency of the RMT signal is about 14 kHz and water can be quite conductive (about 1 ohm-m), hence the boat-towed RMT may not penetrate the water layer at certain sites. In these circumstances, the controlled source is naturally considered to complement the boat-towed RMT data acquisition in order to improve the resolution at depth. Thus, the boat-towed CSRMT approach is for the first time implemented in this study. For the inversion process, two different code packages, EMILIA and MARE2DEM, were used. CSMT and RMT 1D inversions by EMILIA were carried out separately and jointly to analyze galvanic distortions and source effects in the datasets. The resolved distortions and the reality of 2D subsurface structures require using a 2D inversion approach to model the data. Since the plane-wave approximation is satisfied, CSMT data were inverted with RMT 2D inversion code in EMILIA. The plane-wave approximation, however, may cause problems. A real CSMT 2.5D code, MARE2DEM, was therefore used to resolve the fracture zones under the lake. The two results from different inversion codes are then compared, suggesting that MARE2DEM results show better flexibility to model the CSRMT data.

4.3.1 Geological setting and field data acquisition

The detailed geological setting of the study area is given in section 4.2.2. For continuity, only important information is repeated in this section. The aerial map of the study area is shown in Fig. 4.9a. Granitic rocks with diverse types of fracture zones dominate the geology at Äspö (Cosma et al., 2001; Berglund et al., 2003). Most of the fracture zones have been reactivated from older structures depending on their nature (Stanfors et al., 1999). The lake in the study area is connected to the Baltic Sea. The water resistivity in the lake is approximately 1.5 ohm-m according to the direct measurements conducted by Ronczka et al. (2017). The fracture zone NE-1 was expected at the northern side of the profile and was our main target. It is a NE-SW running system about 60 m wide in total (Berglund et al., 2003; Rhén et al., 1997). The NE-1 is highly fractured and hydraulically conductive; it contains both

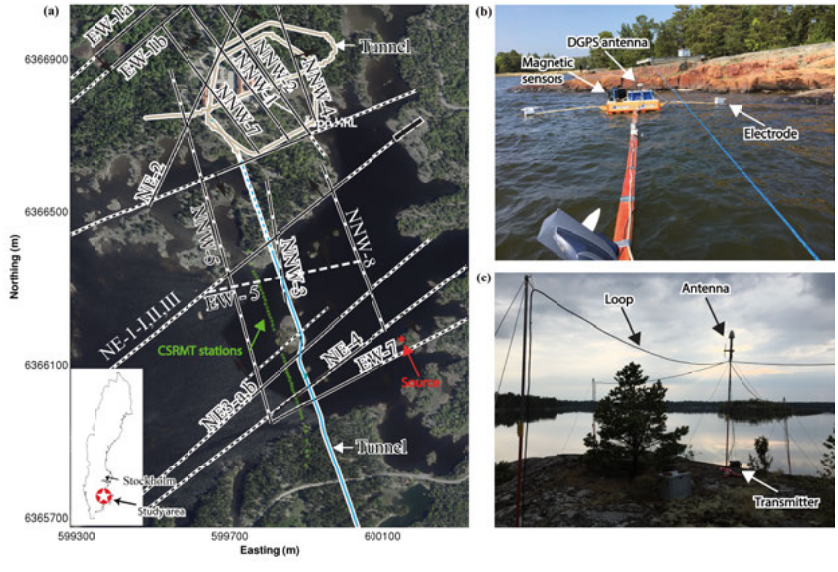

Figure 4.9. (a) Aerial photo of the study area at Äspö HRL site (Image © Google). Green stars in (a) mark the CSRMT and RMT stations, and the source position is shown by a red star. Field photos show (b) the receiver part and setup on the water and (c) double horizontal magnetic dipoles used as the source to generate EM signals. Photos: Shunguo Wang, 2016.

non-saline and brackish water and clay minerals. It is hosted by diorite, fine-grained granite, and greenstone type rocks (Stanfors et al., 1999; Berglund et al., 2003). In addition to the NE-1, three other fracture zones, EW-7, NE-4, and NE-3, exist at the southern side of the profile as shown in Fig. 4.9a (Wikberg et al., 1991; Stanfors et al., 1999; Rhén et al., 1997). The widths of the NE-3 and NE-4 fracture zones are approximately 50 and 40 m, respectively. The EW-5 fracture zone was proposed by Wikberg et al. (1991) and also delineated by our study (Wang et al., 2017a).

As a continuation of the previous study, a boat-towed CSRMT profile was collected at the Äspö HRL site. The previous result using only the RMT dataset (Wang et al., 2017a) motivated using the CSRMT method on the lake in order to better resolve the fracture zones under the 3-6 m deep brackish water. The CSRMT profile and the source position are shown in Fig. 4.9a. The setup of the receiver on the water is shown in Fig. 4.9b. Two horizontal magnetic dipoles generated by two mutually perpendicular loops were used as source during the data acquisition (Fig. 4.9c). The area of each loop is 27 m^2. The maximum current of 20 A together with 5 available windings provided a maximum dipole moment of 2700 Am^2. They were laid out on an island 310 m away from the nearest receiver station and 430 m away from the furthest one (Fig. 4.9a). The selected frequencies for acquisition were 1.25, 2, 4, 6.25, 8, 10, 12.5 kHz in order to resolve deep subsurface structures. Given that this was the first time a boat was used for CSRMT data acquisition, special care was taken to ensure good data quality. The boat was slowly moved by hand along a rope, which was fixed at both ends (Fig. 4.9b), to keep the Enviro-MT system stable on the water even in windy conditions. The boat-towed CSRMT measurement time was longer (~ 8 minutes per station) than the boat-towed RMT measurements. We had to stop and record at each station; for the RMT measurements stopping the boat was not required. In the end, the measurement of 40 CSRMT stations along a 400-m-long profile was achieved within two days. Additionally, eight RMT stations (two on the northern side and six on the southern side of the profile) were surveyed on land to directly estimate the resistivity of the granitic host rock.

4.3.2 1D inversion

Since a controlled source was used in the data acquisition, distortion and source effects should be investigated before using routine 2D algorithms for the inversion of plane-wave data. The CSMT 1D inversion code in EMILIA (Kalscheuer et al., 2015), which accounts for distortion parameters and source effects on CSMT data, was used to invert the electrical resistivity structure along the profile (Fig. 4.10).

Four elements of the impedance tensor were used to do the inversions. The error floor of the impedance tensor is chosen as 5 %. This corresponds to 10 % on apparent resistivity and 2.86 degrees on phase data. Both the CSMT 1D and RMT 1D inversions have reasonable data misfits at about half of the stations. The stitched resistivity models (Figs. 4.10a,b) of the 1D single inversions have better visualization of subsurface structures. The stitched resistivity model (Fig. 4.10c) of joint inversions combines the features from both the CSMT and RMT data. The large distortion parameters (Table 4.4) imply the presence of distortions in the CSMT data. The 2D inversion was considered to better interpret the CSMT and RMT datasets, since part of the distortion can be reduced by doing 2D inversion. Further-

more, the previous study shows that the structures along the profile are mainly 2D.

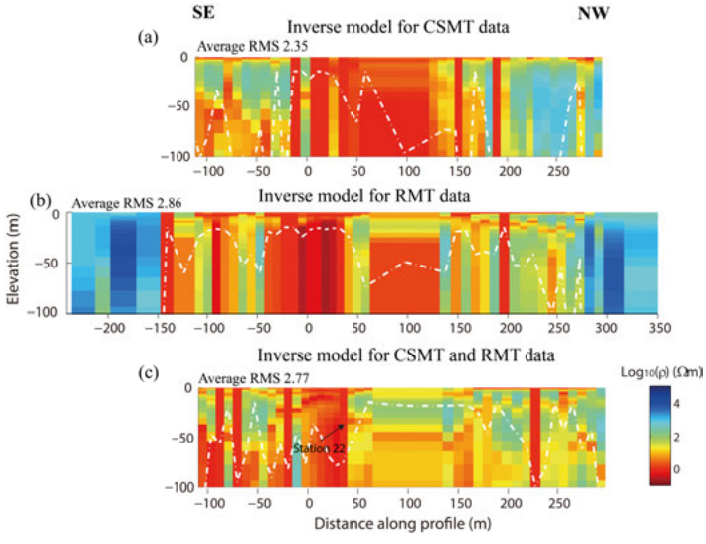

Figure 4.10. (a) The stitched resistivity model of CSMT 1D inversions. (b) The stitched resistivity model of RMT 1D inversions. (c) The stitched resistivity model of the 1D joint inversions of CSMT and RMT data. White dashed line in the models represents exploration depth estimated with the method proposed by Spies (1989).

Table 4.4. *Inverted distortion parameters at station 22 in Fig. 4.10c: four elements for electric field distortions and four elements for magnetic field distortions. The absolute values of distortion parameters for CSMT are larger than the ones for RMT.*

Parameter	P_{xx}	P_{xy}	P_{yx}	P_{yy}	Q_{xx}	Q_{xy}	Q_{yx}	Q_{yy}
CSMT	-0.334	0.010	0.197	-0.596	-0.638	0.486	0.502	0.199
RMT	-0.084	-0.082	0.115	-0.019	0.048	-0.097	0.035	0.060
Joint/CSMT	-0.197	0.006	0.230	-0.502	-0.724	0.465	0.661	0.213
Joint/RMT	-0.435	-0.050	0.071	-0.395	0.029	-0.008	-0.030	0.038

4.3.3 2D inversion based on plane-wave approximation

2D inversion is needed to better resolve detailed structures than 1D inversion. The shortest distance between source and receiver is at least 10 times larger than the skin depth of a 1.25 kHz signal, thus using the 2D RMT inversion code for CSMT data under plane-wave approximation is still appropriate (Bartel and Jacobson, 1987). The input for the inversion is apparent resistivity and phase. An error floor of 10% on apparent resistivity and 5% on phase is used. Fig. 4.11a,b shows the models for single inversions of RMT and CSMT TM-mode data, respectively. Fig. 4.11c,d shows the mod-

els for inversion of CSRMT TM-mode data without and with static shift correction (**Paper III**), respectively.

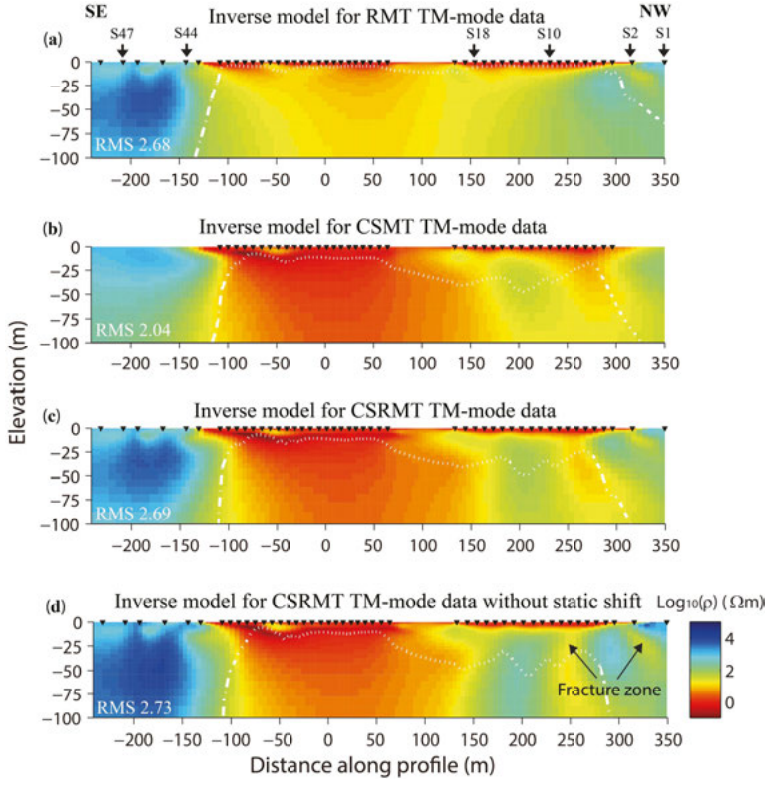

Figure 4.11. Inversion models for (a) RMT TM-mode data, (b) CSMT TM-mode data with plane-wave approximation, (c) CSRMT (including RMT and CSMT) TM-mode data, and (d) CSRMT TM-mode data with static shift correction. The source is at (-310, 0, 2.5) m position. The profile is in *y* direction. All the RMSs are acceptable. Black triangles at the surface represent station positions. White dashed lines in the model present exploration depth calculated with the method proposed by Spies (1989).

High-resistivity features at both ends of the profile correspond to the granitic basement. The bottom of the lake is better resolved in the inversion of CSRMT data (Fig. 4.11c) compared with the inversion of RMT data (Fig. 4.11a). Besides, the conductive zones at 250-350 m distance are more focused in Fig 4.11c than in Fig. 4.11a. The penetration depth of CSMT data should be 2-3 times larger than the one of RMT data theoretically. However, the bedrock below the conductive water layer but shallower than the exploration depth is not resolved (Fig. 4.11b-d). This unreasonable result is possibly due to the non-consideration of the source effect. Thus, 2D inversion with source consideration is needed to invert CSMT data and investigate the unreasonable result.

4.3.4 2D inversion incorporating source effects

A 2.5D inversion of CSMT data is used to evaluate the influence of the plane-wave approximation made for inverting the CSMT data with the RMT inversion code. The code MARE2DEM is used for this purpose. It can use linear or logarithmical apparent resistivity and phase data for MT inversion, and real/imaginary parts, amplitude, and phase of EM fields for CSEM inversion. However, a modification of MARE2DEM is required in order to use the impedance tensor data for the inversion. The instrument Enviro-MT used for data acquisition is unable to record the current of the controlled source, therefore only the impedance tensor data can be used for inversion. Furthermore, 50 wavenumbers from 10^{-5} to 10^{1} m^{-1} equally distributed in logarithmic space are used, in order to run MARE2DEM in high-frequency band (>1 kHz). After the modification, a comparison between 1D and 2D CSMT modelling based on a three-layer model was done to verify the accuracy of the forward modelling. The result shows that both amplitude and phase of the impedance tensor are well modelled by MARE2DEM when the stations are at a certain distance away (> 314 m) from the source (see in **Paper III**).

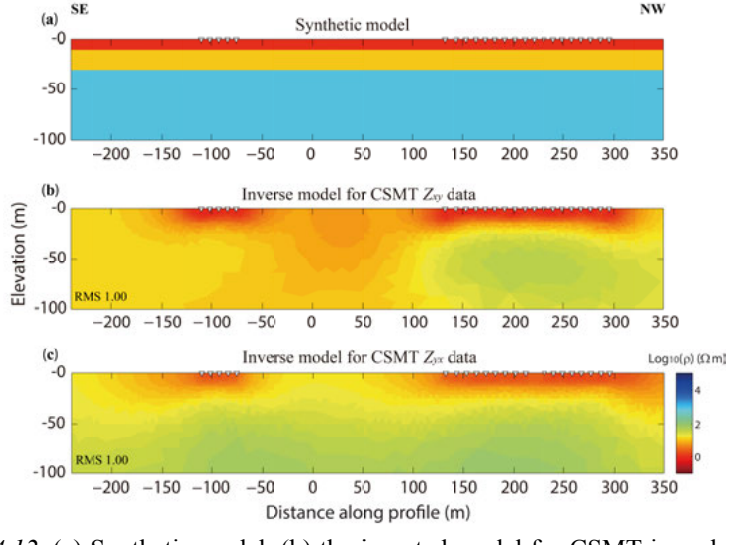

Figure 4.12. (a) Synthetic model, (b) the inverted model for CSMT impedance data Z_{xy}, and (b) the inverted model for CSMT impedance data Z_{yx}. Seven frequencies, 1.25, 2, 4, 6.25, 8, 10, 12.5 kHz, are used in this synthetic test. Receivers are marked with triangles. The magnetic dipole is located at (-310, 0, 2.5) m position. The profile is in *y* direction.

A synthetic test for the 2.5D CSMT inversion is examined before real field data are inverted. The synthetic model is shown in Fig. 4.12a. The source position and frequencies are set equal to the field parameters to generate the synthetic data. Due to the singularity at the source position, no stations are set close to the source. All other stations are the same as in the field.

Gaussian noise (5 %) is added to the synthetic data Z_{xy} and Z_{yx}. The result shows that the inverted model matches the real model below the receiver positions (Fig. 4.12b,c).

After the synthetic test, MARE2DEM was used for inverting field data. The outliers of RMT and CSMT field data were removed due to the diffusive natures of EM fields (Nabighian, 1987). Both single and joint inversions were used to interpret the RMT and CSMT data. The initial model for the inversion was carefully designed. The top part of the model was finely gridded as it represents the target area. The cell size was then increased with depth up to 1.5 times the original size.

The bathymetry data from the previous study close to the CSRMT profile were used to decouple the smoothness along the lake to prevent mapping conductive feature of the saline water into bedrock by smoothness constraint. However, the bathymetry data are not included in the CSMT inversion due to its high sensitivity to inaccurate bathymetry data. The inversion model for

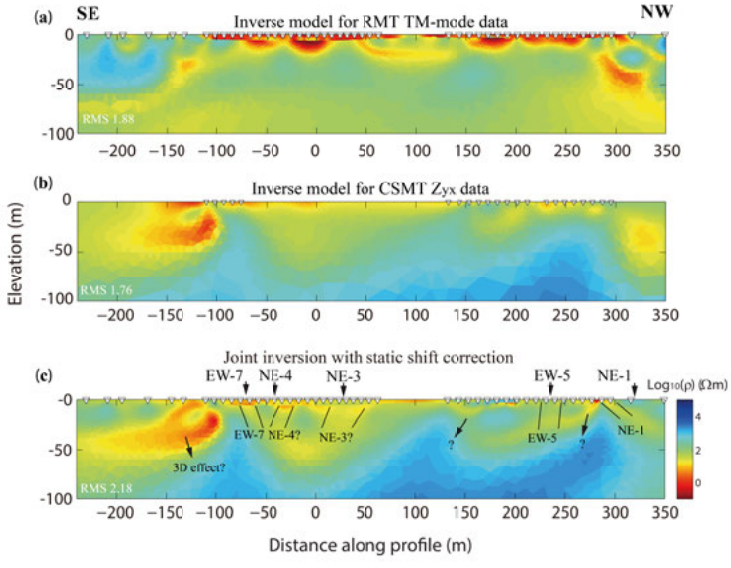

Figure 4.13. (a) Single inversion model for boat-towed RMT TM-mode data, (b) single inversion model for boat-towed CSMT impedance Z_{yx} data, and (c) jointly inverted model for both datasets but with five times more weight on CSMT dataset and with consideration of static shift correction. Triangles are the receiver positions and the source position is not marked for better comparison with the results from EMILIA. Black arrows mark the position of fracture zones mapped from limited borehole and surface observations as well as low resolution seismic data. The source is at (-310, 0, 2.5) m position. The profile is in *y* direction.

the RMT dataset is shown in Fig. 4.13a. The fracture zone NE-1 is resolved at around 300 to 350 m distance along the profile. The lake bottom in the profile is partly visible as a boundary due to the decoupling of the smooth ness constraint. The inversion model for the CSMT dataset is shown in Fig.

4.13b. Due to the source singularity in the modelling, the stations close to the source are not included in the inversion. Three conductive zones are shown in Fig. 4.13b: at -150 to 100 m, 150 to 200 m, and 300 to 350 m distances. In comparison with the RMT inversion, the CSMT inversion gives higher resolution of the details of the subsurface structures. The joint inversion with dataset weighting is shown in Fig. 4.13c. The model in Fig. 4.13c uses five times more weight for the CSMT dataset, since there are less CSMT stations than RMT stations, and CSMT data have higher resolution at depth (Fig. 4.13b). The static shift correction is also used for the RMT dataset in the joint inversion. The subsurface structures in the joint inversion model (Fig. 4.13c) are better resolved compared with both single inversions (Fig. 4.13a,b). All the inversions show good data fit. The fracture zones NE-1, EW-7 and EW-5 are resolved; however, the fracture zones NE-3 and NE-4 cannot be identified with confidence since not enough stations were set above them. The conductive zone at around -150 to -100 m distance may be caused by 3D effect or the high voltage cable buried nearby. Other conductive zones, such as the ones at around 150 m and 275 m distance along the profile, are unclear. A synthetic test based on the interpretation in Fig. 4.13c confirms what have been interpreted (in **Paper III**).

4.3.5 Discussion and conclusions

Boat-towed CSRMT has been implemented and used in mapping fracture zones at Äspö HRL site. The data acquisition was relatively fast compared with standard methods. The CSRMT data have been inverted with different dimensionalities and different consideration of source effect. Apparently, high dimensional inversion creates a better model showing a more detailed structure. The 2D inversion of CSMT data with a proper source consideration better improves the resolution for detecting fracture zones and the bedrock surface compared with the results using the plane-wave approximation. The joint inversion of boat-towed RMT and CSMT data creates a better model than any single inversion.

The implemented boat-towed CSRMT system needs to be upgraded in two aspects. Firstly, the current generated by the controlled source should be recorded. The code MARE2DEM is also able to invert each single component of the EM fields for the resistivity model. Secondly, the results of CSMT data show that the stations close to the source cannot be used for the inversion owing to the singularity of the source and possibly the near source effect. In order to avoid this, an optimized observation system should be designed using 2.5D or 3D modelling with a proper tool before data acquisition.

The boat-towed CSRMT together with the modified inversion code have improved the model resolution and acquisition efficiency in near-surface engineering applications. The improved resolution can help geo-engineers to

distinguish the fracture or weak zones in the bedrock at the shallow water covered area. The improved acquisition efficiency can shorten the planning procedure for the evaluation of infrastructure construction. These implementations, obviously, are not restricted to engineering applications, but geohazards investigation, mineral exploration, and ground water monitoring can benefit from them. Thus, CSRMT could be successfully applied to assist near-surface applications in countries where large areas are covered by shallow waters, such as Sweden, Norway, and Finland.

5 Conclusions and outlook

5.1 Conclusions

To reduce the uncertainty in the model domain, integration and joint inversion of multi-geophysical data should be used. By using these approaches, data coverage of geological target, suppression of field noise, and complementation of sensitivities from different method together improve the resolution of detecting subsurface structures and their underlying physical properties. The three related studies in the thesis clearly demonstrate the advantages of using multi-geophysical methods to improve the model resolution.

RMT, traveltime tomography, reflection seismic, and geotechnical logging together were used at a quick-clay landslide site to better delineate quick clays and their surrounding materials. The results indicate that, as compared with surrounding marine clays, quick clays are more resistive. The quick clays are often found right above the coarse-grained materials in the core logging studies conducted at the site as part of the same project. This combination of quick clays and underlying coarse-grained material produces strong reflectivity and associated with a distinct tomographic character with higher velocity than its surroundings. Thus, this sedimentary sequence comprising quick clays and coarse-grained materials situated within marine clays, yield features with a strong correlation between high velocity and high resistivity. All characterized areas along the survey lines indicate two types of possible landslide scenarios, which will aid in assessment of the risk for future quick-clay landslides.

Joint inversion of the boat-towed RMT and lake-floor ERT data was used in mapping fracture zones at the Äspö HRL. The result not only well resolves a known fracture zone, the NE-1, but also indicates two other conductive zones, which based on poorly documented reports are related to two fracture zones, EW-5 and EW-7. Different weighting techniques and constraints with an *a priori* model yield an improved final model. Data misfit analyses, exploration depth calculation, and model resolution analyses were the three methods used to evaluate the inversion models. Only in this way, the well-constrained part of the model is representative of the subsurface structures. A synthetic test based on the interpretation was used to support the interpretation.

Boat-towed CSRMT method has high efficiency in data acquisition. It was also used for mapping fracture zones at the Äspö HRL to complement the

insufficient resolution of the boat-towed RMT over the saline water environment. The CSRMT data were inverted with different dimensionalities and different considerations of the source effect. Apparently, high dimensional inversion generates a better model, which shows greater detail. The 2D inversion of CSRMT data with a proper source consideration improves the ability to accurately resolve fracture zones and the bedrock level as compared with the results obtained under the plane-wave approximation. Joint inversion of the boat-towed RMT and CSMT provides more detail about subsurface structures than any single inversions. Several fractures zones at the site, including NE-1, EW-5, and EW-7, are resolved based on their conductive nature, while a few others, such as NE-3 and NE-4, need additional confirmation due to insufficient data coverage.

All the studies in the thesis show that integration and joint inversion of multi-geophysical data improve the resolution of the models, which can be used in the planning phase of underground infrastructure (e.g., tunnels or facilities for energy or waste storage) as well as for geohazards investigation. The new implementations in both data acquisition and inversion can also be used for improved results in, for examples, mineral exploration and ground water monitoring.

5.2 Outlook

Although I have improved the resolution of subsurface structures by integration and joint inversion of multi-geophysical data, there are still several areas that can be explored for further improvement.

In the quick-clay investigation, resistivity and velocity models are separately inverted and compared in the interpretation. Even though the models are obtained along the same profiles, the cross-plot of resistivity and velocity could not verify a unique relationship between the two (Fig. 5.1). This may indicate that our models have a structural incompatibility. Therefore, 3D joint inversion of RMT data and seismic traveltime tomography with structural coupling was done to reduce the incompatibility between different models (using a code based on Moorkamp et al., 2011). This research is, however, currently inconclusive and requires further study.

3D inversion has become popular due to the fast development of hardware and parallelization of program (Kelbert et al., 2014; Zhang and Key, 2016). The Earth is in 3D, however, in some particular cases, 2D or even 1D approximation can be used (Kalscheuer et al., 2015). These approximations could, however, always introduce bias in the inversion and will not work in complex environments. Thus, 3D inversion should be used in future research if the cost is acceptable.

The CSRMT data acquisition could be better planned if 2.5D or 3D forward modelling was involved. The optimal observation system can be se-

lected by modelling and then be utilized in the data acquisition. Skipping this step could have serious consequences in a 3D survey with special targets, such as a reservoir or a geothermal plume, in complex environment. Besides, current of the controlled source should be recorded during CSRMT data acquisition. All of these suggestions can help inversion algorithm to obtain a more reliable model of the subsurface.

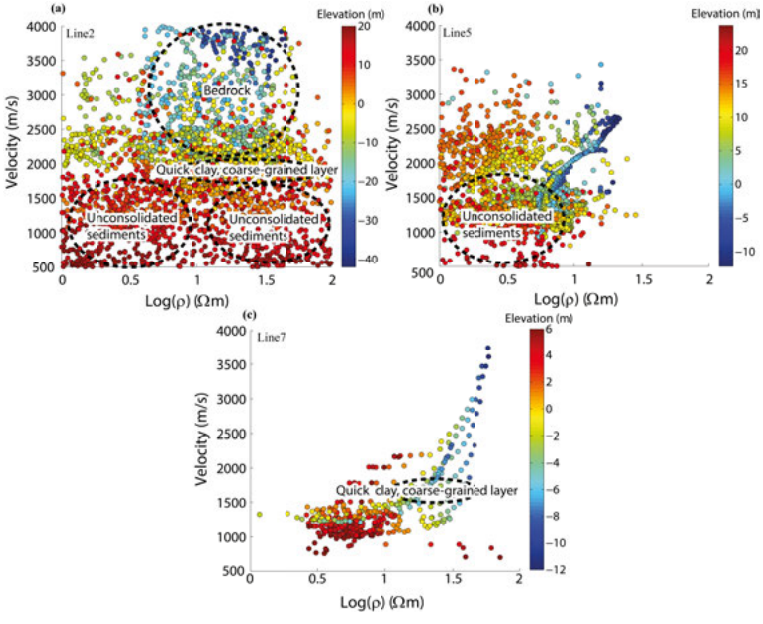

Figure 5.1. The relationship between resistivity and velocity along (a) line 2, (b) line 5, and (c) line 7 in **Paper I**. The resistivity and velocity models were inverted separately.

Transient electromagnetics (TEM) is not influenced by the near-source effect, which is also suitable for resolving conductors. Thus, boat-towed TEM could also be implemented. This new implementation together with boat-towed RMT, boat-towed CSRMT, and lake-floor ERT would be capable of further improving the resolution of mapping conductive fracture zones, such as those at the Äspö HRL. This could be a new efficient and effective tool in near-surface applications for geo-engineering purposes.

"All models are wrong but some are useful (Box, 1979)". This aphorism is also suitable in geophysics (Constable et al., 2015). In order to guarantee the results in **Paper II**, hundreds of inversions were performed, resulting in a number of models that fit the datasets with a reasonable level of acceptance. Only a few of those models were, however, finally selected to show in **Paper II**. Therefore, model fusion or model statistics of all the accepted models can be used in the future to further reduce the model uncertainty.

6 Summary in Swedish

Geofysiska mätningar är icke-förstörande men är samtidigt effektiva för att skaffa information om strukturer och fysikaliska egenskaper hos geologin under markytan. En av de största utmaningarna är att geofysiska modeller generellt ej är unika. Flera olika modeller passar och kan lika bra förklara ett dataset. Vidare är mätningarnas upplösning och brusnivån vid datainsamling begränsande för hur exakt de fysikaliska egenskaperna av geologin kan modelleras. Dessa utmaningar har gjort att geofysiker under flera decennier har gjort stora insatser för att kunna skapa modeller som så exakt som möjligt beskriver de fysikaliska egenskaperna hos geologin. Joint inversion och integrering av flera geofysiska dataset är två angreppssätt som jag har tillämpat i mina studier för att förbättra upplösningen av geologiska strukturer. Tillsammans med implementeringen av ny hårdvara för datainsamling och nyutvecklad mjukvara för inversion av insamlat data, har jag använt dessa två angreppssätt i min forskning med fokus på ytnära tillämpningar.

I denna avhandling har radio-magnetotelluriska mätningar (RMT), båtbogserad RMT med kontrollerad källa (CSRMT), elektrisk resistivitetstomografi (ERT), och seismisk gångtidstomografi valts ut och använts tillsammans för undersökningar av kvicklera och detektering av sprickzoner på platser som täcks av grundare sjöar och vattendrag. Inversion där flera olika geofysiska metoder kombineras är bättre för att avbilda geologin än metoder som bara använder en geofysisk metod. Genom att till exempel kombinera och invertera sjöbotten-ERT och båtbogserad RMT är sprickzoner bättre avbildade och detta med högre noggrannhet. Genom att utföra CSRMT-mätningar och RMT-mätningar genom att bogsera utrustningen med en båt och sedan utföra en kombinerad inversion kan strukturer i berggrunden, i synnerhet på större djup, beskrivas med högre upplösning än om varje dataset inverteras var för sig.

Under mina doktorandstudier har två nya metoder att mäta implementerats. (1) Båtbogserad CSRMT-mätning implementerades för att vidareutveckla RMT- och CSRMT-metoderna till att inte bara innefatta landmätningar utan också tillämpningar på grunt vatten. Detta är viktigt eftersom storskaliga infrastruktursprojekt ofta passerar under områden med vatten (till exempel flerspåriga tåg- och biltunnlar såsom Förbifart Stockholm). (2) Modifikationer av den välstrukturerade EMILIA-koden tillåter kombinerad inversion av båtbogserad RMT och sjöbotten-ERT och med hjälp av modifikationer av den likaså välstrukturerade MARE2DEM-koden kan högupplöst modellering av högfrekvent CSRMT-data utföras. Med den modifierade MARE2DEM-

koden kan vidare båtbogserad RMT- och CSRMT-data kombineras vid inversion. Modifikationerna av EMILIA- och MARE2DEM-koderna är en annan typ av nya implementeringar som garanterar framgångsrika mätningar för ytnära RMT- och CSRMT-tillämpningar.

Studier som jag genomfört under min doktorandtid är en del av projektet TRUST (TRansparent Underground STructure) och ska vara användbara för ytnära tillämpningar, till exempel för planering av infrastruktur under jord, karaktärisering av bergmassa för energi- och avfallslagring, och för riskbedömning för katastrofer relaterade till geologi. I kapitel 4 i avhandlingen illustreras detta med tre ytnära tillämpningar i tre artiklar.

I den första artikeln (**Paper I**) användes RMT och seismisk gångtidstomografi i kombination för att kartera kvicklera och strukturer där kvicklera finns. Studien var en del av ett SEG-GWB-projekt (SEG, 2017). Kvicklera och jordskred där kvicklera är inblandade, vilka bland annat förekommer i Norden och i norra Nordamerika, är en av de allvarligaste så kallade geo-riskerna och är därför viktigt att beforska. Forskningslokalen där vi gjorde mätningar är belägen strax norr om Lilla Edet längs med Göta Älv. Resultaten från RMT-mätningarna visar att resistiviteten på möjliga kvickleror (10-100 ohm-meter) är högre än omkringliggande marina leror som håller en resistivitet på 1-10 ohm-meter. Resultaten från gångtidstomografin visar relativt hög seismisk hastighet i kvicklera och även i ett underliggande sandlager. Genom att kombinera RMT-data och seismisk gångtidstomografi och även använda information från borrhål lyckades vi kartera och bestämma placeringen av möjliga zoner med kvicklera samt presentera tänkbara jordskredsscenarier.

I den andra artikeln (**Paper II**) används kombinerad inversion av data från båtbogserad RMT och sjöbotten-ERT för att kartera sprickzoner vid Äspö Hard Rock Laboratory i Oskarshamn. Studien var en del av TRUST-projektet (TRUST, 2016), som hade till syfte att förbättra upplösningen vid användning av flera geofysiska metoder kombinerade för ytnära tillämpningar i framförallt urbana miljöer. Data från mätningarna av båtbogserad RMT och sjöbotten-ERT kombinerades för inversion med en modifierad version av EMILIA-koden (Kalscheuer et al., 2010, Wang et al., 2017a). Den inverterade resistivitetsmodellen visar inte bara den kända sprickzonen utan också en annan som endast antytts vid tidigare studier. Resultatet demonstrerar tydligt fördelen med att använda den nya implementeringen både för datainsamling och inversion i syfte att förbättra upplösningen vid ytnära tillämpningar.

I den sista artikeln (**Paper III**) genomfördes inversion av en kombination av båtbogserad RMT och CSRMT för att kartera samma sprickzoner som i **Paper II**. Tvådimensionell inversion av båtbogserad CSRMT-data gjordes separat med både EMILIA-koden (Kalscheuer et al., 2008) som antar att det är plana vågor och med MARE2DEM-koden (Key, 2016) som helt tar hänsyn till källans effekt. Resultaten från MARE2DEM föreslår fler strukturer och fler möjliga sprickzoner än EMILIA-koden. Inversion med

MARE2DEM där båtbogserad RMT-data och CSRMT-data kombineras visar också fler detaljer av både sprickzoner och berggrundsytan än någondera av inversionerna med enskilda dataset. Denna studie föreslår också att noggrann simulering skall göras före fältarbeten för att kunna designa optimal geometri på uppställningen av instrument, detta för att undvika effekter av att källan är för nära.

Acknowledgements

Almost four years of study in Uppsala gives me a lot of new ideas and innovational knowledge. All these are achieved with great help from my supervisors, friends, colleagues, and my families.

Alireza Malehmir is the first one who I would like to sincerely appreciate. He is the one who opens a door to a new life for me. Without him I would not start my study at UU. He helps me to solve registration problem together with Fatima. As main advisor he has intentionally trained me from many aspects, such as writing, teaching, data acquisition, interpretation, data processing, presentation, etc. With a great effort he enlightened me in the seismic world, which lets me understand more about seismic traveltime tomography and reflection method. When we were in the field or conference together, he made the atmosphere enjoyable.

Mehrdad Bastani as one of my co-supervisors is sincerely appreciated. He dedicates a lot of effort to help me not only in my research but also in my life. He guided me intelligently and peacefully no matter what kind of mess I had. He transferred his EM knowledge to me with great patience. We discussed my research results, manuscript, and future plans many times in his office, even with limited time provided to him at SGU. We together collected field data many times with joy. When I felt hurt in my knee in the field, he took over most of the work with pleasure. When I had hard time to understand my situation, he analyzed it clearly to me and helped me to end the hard time.

Thomas Kalscheuer as one of my co-supervisors is also sincerely appreciated. He dedicates a lot of effort in my research. He is a great contributor for EM data inversion in my study. The new version of EMILIA is frequently shared from him to me. The moment of sitting together to plan joint inversion approach and modify the code is really joyful for me. He supervises me with prudence in making results. The correction for my manuscript from him is with super carefulness. Teaching opportunities to me are kindly provided by him too. All the training from him makes me have better judgments of how to be a professional EM geophysicist.

Steven Constable is given my special thanks for hosting me when I am at Scripps Institution of Oceanography (SIO). He puts great energy to supervise me when I finalize my research. The routine meeting on Fridays is surprisingly helpful. We discuss what I have done, what my questions are, and what I should do. The commercial computation resource provided by him guaran-

tees my research progress. Without his great help, the final stage of my PhD would not go smoothly.

Laust Perdersen and Christopher Juhlin are much appreciated. Laust and I had several discussions, which gave me very useful guide. Many friends asked me why I chose Uppsala, the answer is: Laust works here. I will solely miss him. Chris also helps me in the research and life in Uppsala. In the dark time of every year, party at his home gives me extra motivation to focus on study. Jochen Kamn (my mentor), Chunling Shan, and María García Juanatey are appreciated for helpful discussions and showing me EM knowledge. Fengjiao Zhang and Ari Tryggvason are appreciated for helping me to learn 3D tomography. I also thank Lars Dynesius, Torleif Dahlin, Lena Persson, Alexandross Savvaidis, Naser Meqbel, Hans Palm for the collaboration we had. Kerry Key and Chloe Gustafson are thanked for helping me to solve the problem when I run MARE2DEM. Special thanks to Magnus and Peter who translated and modified the Swedish summary for this thesis, and they together with Silvia, Fredric, Bojan, Georgiana, Chloe and Daniel(SIO) polished my thesis, thank you all. I also thank Alex for patiently teaching me Swedish.

Jishan He, Shikun Dai, Qiyun Jiang, Jingbo Wen are specially appreciated. Without the supporting from you, I could not make the trip so far. I enjoyed the moment every time I visited you in Changsha. Bin Xiong is thanked for the helpful discussions and the constructive suggestions via telephone talks.

Max Moorkamp and Anna Avdeeva are appreciated for warmly hosting me at University of Leicester to learn 3D joint inversion of seismics and MT.

I would like to thank Rémi, Suman, Monika, Angela, Sebastian, Iwona, Rūta, Marta, Nada, Joao, Dragos, Joachim, Théo, Daniel, Claudia, Tegan, Azita, Emil, Garðar, Svenja, Chris, Joanna, Darina, Sahar, Zeynab, Babis, Livsa, Haber, Omid, Bjarne, Möhsen, Hamzeh, Samar, Ka Lok and others for the fun we had together at the department, nations, among others. These memories will stay with me forever.

Special thanks to Lichuan, Fei, Haizhou for the fun, dinners, sports and no-sleep nights we had together. I also thank other Chinese friends met in my PhD time: Feiyan, Hongling, Changqing, Xiao, Ping, Na, Zhou(SIO), Yuxiang(SIO), Hong(SIO), Zhibin, Liang, Lebing, Keqiang, Le, Zhina, Fan, Lei, Meiyuan, Weijia, Wenxing, Jiajie, Fengzhen, Liguo, Wei(SIO), Bing(SIO), Rui, Ge, Xiaoou, Fengyi, Yongmei, Zhiliang, Yaocen, Xiaodong, Ruixue and others. Thank you all for happy memories we shared.

I appreciate the China Scholarship Council (201306370039), Formas (25220121907), BeFo (project 340), SBUF-Skanska, National Natural Science Foundation of China (D040901) and National High Technology Research and Development Program of China (2012AA09A20105) for supporting my PhD study at UU and the Byzantine travel scholarship for supporting around half year of my PhD study at SIO. Besides, EMIW, EAGE, V-dala

Nation are also thanked for partly supporting my attendance of international workshops and conference.

Last but not the least, my parents are deeply appreciated, without their all kinds of support and encouragement on the way to my PhD, I definitely would not make it. All other family members as well as friends in China are also thanked: all of you help me to become stronger. The way ahead is long; I see no ending, yet up and down I will search with my will unbending.

Shunguo Wang, San Diego, August 2017

References

AB Svensk Filmindustri, 1957. Veckorevy 1957-06-12, SVT. Available from: http://www.filmarkivet.se/sv/Film/?movieid=336 [21 January 2016]

Abubakar, A., Gao, G., Habashy, T.M. and Liu, J., 2012. Joint inversion approaches for geophysical electromagnetic and elastic full-waveform data. *Inverse Problems*, **28**(5), p.055016.

Aiken, C.L., Hastings, D.A. and Sturgul, J.R., 1973. Physical and computer modeling of induced polarization. *Geophys. Prospect.*, **21**(4), 763-782.

Almén, K.E. and Stenberg, L., 2005. *Äspö Hard Rock Laboratory. Characterisation methods and instruments. Experiences from the construction phase* (No. SKB-TR-05-11), Swedish Nuclear Fuel and Waste Management Co..

Andersson-Sköld, Y., Rankka, K., Lind, B., Ode´n, K.,Torrance, J.K., Stevens, R.L., Dahlin T., Leroux V., 2005. Quick clay6An investigation in Southwest Sweden. In: Senneset, Flaate and Larsen (eds) *Landslides and Avalanches*: ICFL 2005 Norway. Taylor and Francis Group, London.

Bartel, L.C. and Jacobson, R.D., 1987. Results of a controlled-source audiofrequency magnetotelluric survey at the Puhimau thermal area, Kilauea Volcano, Hawaii. *Geophysics*, **52**(5), 665-677.

Bastani, M., 2001. EnviroMT- *A New Controlled Source/Radio Magnetotelluric System*. Ph.D. thesis, Uppsala University, Uppsala.

Bastani M., Hübert J., Kalscheuer T., Pedersen L.B., Godio A. and Bernard J., 2012. 2D joint inversion of RMT and ERT data versus individual 3D inversion of full tensor RMT data: An example form Trecate site in Italy. *Geophysics*, **77**(4), WB233-WB243.

Bastani, M. and Pedersen, L.B., 2001. Estimation of magnetotelluric transfer functions from radio transmitters. *Geophysics*, **66**(4), 1038-1051.

Bastani, M., Persson L., Mehta S. and Malehmir A., 2015. Boat-towed radiomagnetotellurics-A new technique and case study from the city of Stockholm. *Geophysics*, **80**(6), B193-B202.

Berglund, J., Curtis, P., Eliasson, T., Olsson, T., Starzec, P. and Tullborg, E.L., 2003. *Äspö Hard Rock Laboratory. Update of the geological model 2002*. Swedish Nuclear Fuel and Waste Management Co..

Benz, H.M., Chouet, B.A., Dawson, P.B., Lahr, J.C., Page, R.A., Hole, J.A., 1996. Three dimensional P- and S-wave velocity structure of Redoubt Volcano, Alaska. *J. Geophy. Res.*, **101**, 8111-8128.

Box, G.E., 1979. Robustness in the strategy of scientific model building. *Robustness in statistics*, **1**, 201-236.

Brodic, B., Malehmir, A., Juhlin, C., Dynesius, L., Bastani, M. and Palm, H., 2015. Multicomponent broadband digital-based seismic landstreamer for near-surface applications. *J. Appl. Geophys.*, **123**, 227-241.

Candansayar M.E. and Tezkan B., 2008. Two-dimensional joint inversion of radiomagnetotelluric and direct current resistivity data. *Geophys. Prospect.*, **56**(5), 737-749.

Coggon, J.H., 1971. Electromagnetic and electrical modeling by the finite element method. *Geophysics*, **36**(1), 132-155.
Constable, S.C., Parker, R.L. and Constable, C.G., 1987. Occam's inversion: A practical algorithm for generating smooth models from electromagnetic sounding data. *Geophysics*, **52**(3), 289-300.
Constable, S., Orange, A. and Key, K., 2015. And the geophysicist replied: "Which model do you want?". *Geophysics*, **80**(3), E197-E212.
Coutant, O., Bernard, M.L., Beauducel, F., Nicollin, F., Bouin, M.P. and Roussel, S., 2012. Joint inversion of P-wave velocity and density, application to La Soufrière of Guadeloupe hydrothermal system. *Geophys. J. Int.*, **191**(2), 723-742.
Cosma, C., Olsson, O., Keskinen, J. and Heikkinen, P., 2001. Seismic characterization of fracturing at the Äspö Hard Rock Laboratory, Sweden, from the kilometer scale to the meter scale. *Int. J. Rock Mech. Min. Sci.*, **38**(6), 859-865.
Dahlin, T. and Zhou, B., 2006. Multiple-gradient array measurements for multichannel 2D resistivity imaging. *Near Surf. Geophys.*, **4**(2), 113-123.
Daily, W., Ramirez, A., Binley, A., LaBrecque, D., 2005. *Electrical Resistance Tomography - Theory and Practice*, in Butler (2005), chapter 17, 525-550.
deGroot-Hedlin, C. and Constable, S., 1990. Occam's inversion to generate smooth, two-dimensional models from magnetotelluric data. *Geophysics*, **55**(12), 1613-1624.
Dey, A. and Morrison, H.F., 1979. Resistivity modelling for arbitrarily shaped two-dimensional structures. *Geophys. Prospect.*, **27**(1), 106-136.
Donohue, S., Long, M., O'Connor, P., Eide-Helle, T., Pfaffhuber, A.A., Rømoen, M., 2012. Multi-method mapping of quick-clay. *Near Surf. Geophys*. **10**(3), 207-219.
Eaton, D.W., 1999. Weak elastic-wave scattering from massive sulfide orebodies. *Geophysics*, **64**(1), 289-299.
Edwards, L.S., 1977. A modified pseudosection for resistivity and IP. *Geophysics*, **42**(5), 1020-1036.
Everett, M.E., 2013. *Near-surface applied geophysics*. Cambridge University Press.
Gallardo, L.A. and Meju, M.A., 2003. Characterization of heterogeneous near‐surface materials by joint 2D inversion of dc resistivity and seismic data. *Geophys. Res. Lett.*, **30**(13), 1658.
Gallardo, L.A. and Meju, M.A., 2004. Joint two‐dimensional DC resistivity and seismic travel time inversion with cross‐gradients constraints. *J. Geophys. Res.: Solid Earth*, **109**(B3).
Gallardo, L.A. and Meju, M.A., 2007. Joint two-dimensional cross-gradient imaging of magnetotelluric and seismic traveltime data for structural and lithological classification. *Geophys. J. Int.*, **169**(3), 1261-1272.
Gallardo, L.A. and Meju, M.A., 2011. Structure‐coupled multiphysics imaging in geophysical sciences. *Rev. Geophys.*, **49**(1).
Haber, E. and Gazit, M.H., 2013. Model fusion and joint inversion. *Surv. Geophys.*, **34**(5), 675-695.
Goldstein, M.A. and Strangway, D.W., 1975. Audio-frequency magnetotellurics with a grounded electric dipole source. *Geophysics*, **40**(4), 669-683.
Groom, R.W. and Bahr, K., 1992. Corrections for near surface effects: decomposition of the magnetotelluric impedance tensor and scaling corrections for regional resistivities: a tutorial. *Surv. Geophys.*, **13**(4), 341-379.
Hohmann, G.W., 1971. Electromagnetic scattering by conductors in the earth near a line source of current. *Geophysics*, **36**(1), 101-131.
Hu, W., Abubakar, A. and Habashy, T.M., 2009. Joint electromagnetic and seismic inversion using structural constraints. *Geophysics*, **74**(6), R99-R109.

Huang, H., 2005. Depth of investigation for small broadband electromagnetic sensors. *Geophysics*, **70**(6), G135-G142.

Iyer, H.M. and Hirahara, K. eds., 1993. *Seismic tomography: Theory and practice*. Springer Science & Business Media.

Julia, J., Ammon, C.J., Herrmann, R.B. and Correig, A.M., 2000. Joint inversion of receiver function and surface wave dispersion observations. *Geophys. J. Int.*, **143**(1), 99-112.

Jones, A.G. and Groom, R.W., 1993. Strike-angle determination from the magnetotelluric impedance tensor in the presence of noise and local distortion: rotate at your peril!. *Geophys. J. Int.*, **113**(2), 524-534.

Kalscheuer, T., Pedersen, L.B., Siripunvaraporn, W., 2008. Radiomagnetotelluric two-dimensional forward and inverse modelling accounting for displacement currents. *Geophys. J. Int.*, **175**(2), 486-514.

Kalscheuer, T., García Juanatey M.A., Meqbel N., Pedersen L.B., 2010. Non-linear model error and resolution properties from two-dimensional single and joint inversions of direct current resistivity and radiomagnetotelluric data. *Geophys. J. Int.*, **182**(3), 1174-1188.

Kalscheuer, T., Hübert, J., Kuvshinov, A., Lochbühler, T. and Pedersen, L.B., 2012. A hybrid regularization scheme for the inversion of magnetotelluric data from natural and controlled sources to layer and distortion parameters. *Geophysics*, **77**(4), E301-E315.

Kalscheuer, T., Bastani, M., Donohue, S., Persson, L., Pfaffhuber, A.A., Reiser, F., and Ren, Z.Y., 2013. Delineation of a quick clay zone at Smørgrav, Norway, with electromagnetic methods under geotechnical constraints. *J. Appl. Geophys.*, **92**, 121-136.

Kalscheuer, T., Blake, S., Podgorski, J.E., Wagner, F., Green, A.G., Maurer, H., Jones, A.G., Muller, M., Ntibinyane, O. and Tshoso, G., 2015. Joint inversions of three types of electromagnetic data explicitly constrained by seismic observations: results from the central Okavango Delta, Botswana. *Geophys. J. Int.*, **202**(3), 1429-1452.

Kelbert, A., Meqbel, N., Egbert, G.D. and Tandon, K., 2014. ModEM: a modular system for inversion of electromagnetic geophysical data. *Comput. Geosci.*, **66**, 40-53.

Key, K. and Ovall, J., 2011. A parallel goal-oriented adaptive finite element method for 2.5-D electromagnetic modelling. *Geophys. J. Int.*, **186**(1), 137-154.

Krawczyk, C. M., Polom, U., Malehmir, A., Bastani, M., 2013. Quick-clay landslides in Sweden – insights from shear-wave reflection seismics and geotechnical integration. *Near Surface Geoscience, 19th EAGE European Meeting of Environmental and Engineering Geophysics*, Bochum.

Li, Y. and Key, K., 2007. 2D marine controlled-source electromagnetic modeling: Part 1—An adaptive finite-element algorithm. *Geophysics*, **72**(2), WA51-WA62.

Lines, L.R., Schultz, A.K. and Treitel, S., 1988. Cooperative inversion of geophysical data. *Geophysics*, **53**(1), 8-20.

Loke, M.H., 1999. Electrical imaging surveys for environmental and engineering studies. A practical guide to 2-D and 3-D surveys.

Loke M.H., 2002. Rapid 2D resistivity forward modelling using the finite-difference and finite-element methods. *www.geoelectrical.com*.

Long, M., Donohue, S., L'Heureux, J.-S., Solberg, I.-L., Rønning, J.S., Limacher, R., O'Connor, P., Sauvin, G., Rømoen, M., Lecomte, I., 2012. Relationship between electrical resistivity and basic geotechnical parameters for marine clays. *Can. Geotech. J.*, **49**(10), 1158-1168.

Malehmir, A., Andersson, M., Mehta, S., Brodic, B., Munier, R., Place, J., Maries, G., Smith, C., Kamm, J., Bastani, M. and Mikko, H., 2016. Post-glacial reactivation of the Bollnas fault, central Sweden: a multidisciplinary geophysical investigation. *Solid Earth*, **7**(2), 509-527.

Malehmir, A., Bastani, M., Krawczyk, C., Gurk, M., Ismail, N., Polom U., Persson, L., 2013a. Geophysical assessment and geotechnical investigation of quick-clay landslides - a Swedish case Study. *Near Surf. Geophys.*, **11**(3), 341-350.

Malehmir, A., Saleem, M.U., Bastani, M., 2013b. High-resolution reflection seismic investigations of quick-clay and associated formations at a landslide scar in southwest Sweden. *J. Appl. Geophys.*, **92**, 84-102.

Malehmir, A., Socco, L.V., Bastani, M., Krawczyk, C.M., Pfaffhuber, A.A., Miller, R.D., Maurer, H., Frauenfelder, R., Suto, K., Bazin, S. and Merz, K., 2016. Chapter Two-Near-Surface Geophysical Characterization of Areas Prone to Natural Hazards: A Review of the Current and Perspective on the Future. *Adv. Geophys.*, **57**, 51-146.

Makurat, A., Løset, F., Hagen, A.W., Tunbridge, L., Kveldsvik, V. and Grimstad, E., 2006. *A descriptive rock mechanics model for the 380–500 m level*. Report R-02-11, Swedish Nuclear Fuel and Waste Management Co..

Mehta, S., Bastani, M., Malehmir, A. and Pedersen, L.B., 2017a. Resolution and sensitivity of boat-towed RMT data to delineate fracture zones–Example of the Stockholm bypass multi-lane tunnel. *J. Appl. Geophys.*, **139**, 131-143.

Mehta, S., Bastani, M., Malehmir, A., and Pedersen, L.B., 2017b. CSRMT survey on frozen lake – A new technique with an example from the Stockholm bypass tunnel. *EAGE Near Surface Geoscience*, Malmö-Sweden.

Menke, W., 1989. *Geophysical data analysis: discrete inverse theory*, Vol. 45 of International Geophysics Series, Academic Press, London.

Moorkamp, M., Heincke, B., Jegen, M., Roberts, A.W. and Hobbs, R.W., 2011. A framework for 3-D joint inversion of MT, gravity and seismic refraction data. *Geophys. J. Int.*, **184**(1), 477-493.

Moorkamp, M., Jones, A.G. and Fishwick, S., 2010. Joint inversion of receiver functions, surface wave dispersion, and magnetotelluric data. *J. Geophys. Res.: Solid Earth*, **115**(B4).

Moorkamp M., Lelievre P.G., Linde N., Khan A., 2016. *Integrated imaging of the earth*. Wiley Press.

Nabighian, M.N., 1988. *Electromagnetic methods in applied geophysics—Theory (Volume 1)*. Society of Exploration Geophysicists, Tulsa, OK.

Nadim F., Pedersen, S.A.S., Schmidt-Thomé, P., Sigmundsson, F., Engdahl, M., 2008. Natural hazards in Nordic Countries. *Episodes*, **31**(1), 176-184.

Nolet, G., 1987. *Seismic wave propagation and seismic tomography. In Seismic tomography* (p.1-23). Springer Netherlands.

Paige, C.C., Saunders, M.A., 1982. LSQR: An algorithm for sparse linear equations and sparse least squares. *ACM Trans. Math. Softw.*, **8**(1), 43-71.

Pedersen, L.B., Bastani, M., Dynesius, L., 2006. Some characteristics of the electromagnetic field from radiotransmitters in Europe. *Geophysics*, **71**(6), 279-284.

Pedersen, L.B., Bastani, M. and Dynesius, L., 2005. Groundwater exploration using combined controlled-source and radiomagnetotelluric techniques. *Geophysics*, **70**(1), G8-G15.

Pedersen, L.B., Engels, M., 2005. Routine 2D inversion of magnetotelluric data using the determinant of the impedance tensor. *Geophysics*, **70**(2), G33-G41.

Podvin, P., Lecomte, I., 1991. Finite difference computation of traveltimes in very contrasted velocity models: a massively parallel approach and its associated tools. *Geophys. J. Int.*, **105**(1), 271-284.

Pratt, R.G., 1999. Seismic waveform inversion in the frequency domain, Part 1: Theory and verification in a physical scale model. *Geophysics*, **64**(3), 888-901.

Rankka, K., Andersson-Sköld, Y., Hultén, C., Larsson, R., Leroux, V., Dahlin, T., 2004. *Quick-clay in Sweden*. Swedish Geotechnical Institute, technical report number 65, 137, Linköping.

Rhén, I., Gustafsson, G., Stanfors, R. and Wikberg, P., 1997. *Äspö HRL-Geoscientific evaluation 1997/5. Models based on site characterization 1986-1995* (No. SKB-TR-97-06), Swedish Nuclear Fuel and Waste Management Co..

Rodi, W. and Mackie, R.L., 2001. Nonlinear conjugate gradients algorithm for 2-D magnetotelluric inversion. *Geophysics*, **66**(1), 174-187.

Ronczka, M., Hellman, K., Günther, T., Wisén, R. and Dahlin, T., 2017. Electric resistivity and seismic refraction tomography: a challenging joint underwater survey at Äspö Hard Rock Laboratory. *Solid Earth*, **8**(3), 671-682.

Salas-Romero, S., Malehmir, A., Snowball, I., Lougheed, B.C. and Hellqvist, M., 2016. Identifying landslide preconditions in Swedish quick clays—Insights from integration of surface geophysical, core sample-and downhole property measurements. *Landslides*, **13**(5), 905-923.

Schlumberger, M., 1939. The application of telluric currents to surface prospecting. *Eos, Transactions American Geophysical Union*, **20**(3), 271-277.

SEG, 2017. http://seg.org/About-SEG/Geoscientists-Without-Borders.

Shan C., Bastani, M., Malehmir, A., Persson, L., Engdahl, M., 2014. Integrated 2D modeling and interpretation of geophysical and geotechnical data to image quick-clays at a landslide site in southwest Sweden. *Geophysics*, **79**(4), EN61-EN75.

Shan C., Bastani M., Malehmir A., Persson L., Lundberg E., 2016. Integration of controlled-source and radio magnetotellurics, electric resistivity tomography, and reflection seismics to delineate 3D structures of a quick-clay landslide site in southwest of Sweden. *Geophysics*, **81**(1), B13-B29.

Silvester, P.P. and Ferrari, R.L., 1996. *Finite elements for electrical engineers*. Cambridge University Press.

Stanfors, R., Rhén, I., Tullborg, E.L. and Wikberg, P., 1999. Overview of geological and hydrogeological conditions of the Äspö hard rock laboratory site. *Appl. Geochem.*, **14**(7), 819-834.

Siripunvaraporn, W., Egbert, G., 2000. An efficient data-subspace inversion method for 2Dmagnetotelluric data. *Geophysics*, **65**(3), 791–803.

Siripunvaraporn, W., Egbert, G., Lenbury, Y. and Uyeshima, M., 2005. Three-dimensional magnetotelluric inversion: data-space method. *Phys. Earth Planet. In.*, **150**(1), 3-14.

Solberg, I., 2007. *Geological, geomorphological and geophysical investigations of areas prone to clay slides: examples from Buvika, Mid Norway*. Ph.D. thesis. Norwegian University of Science and Technology, Trondheim.

Solberg, I., Hansen, L., Rønning, J.S., Haugen, E.D., Dalsegg, E., Tønnesen, J.F., 2012. Combined geophysical and geotechnical approach to ground investigations and hazard zonation of a quick-clay area, mid Norway. *Bull. Eng. Geol. Environ.*, **71**(1), 119-133.

Spies, B.R., 1989. Depth of investigation in electromagnetic sounding methods. *Geophysics*, **54**(7), 872-888.

Swift C.M. Jr. 1967. *A magnetotelluric investigation of an electrical conductivity anomaly in the South Western United States*, PhD thesis, Massachusetts Institute of Technology, Cambridge.

Tezkan, B., Goldman, M., Greinwald, S., Hördt, A., Müller, I., Neubauer, F.M. and Zacher, G., 1996. A joint application of radiomagnetotellurics and transient electromagnetics to the investigation of a waste deposit in Cologne (Germany). *J. Appl. Geophys.*, **34**(3), 199-212.

Tikhonov, A.N., Arsenin, V.I. and John, F., 1977. *Solutions of ill-posed problems* (Vol. 14). Washington, DC: Winston.

TRUST, 2016. http://trust-geoinfra.se/, accessed 20 July 2016.

Tryggvason, A. and Linde, N., 2006. Local earthquake (LE) tomography with joint inversion for P‐ and S‐wave velocities using structural constraints. *Geophys. Res. Lett.*, **33**(7).

Tryggvason, A., Rögnvaldsson, S.Th., Flóvenz, Ó.G., 2002. Three-dimensional imaging of the P- and S-wave velocity structure and earthquake locations beneath Southwest Iceland. *Geophys. J. Int.*, **151**(3), 848-866.

Turberg, P., Müller, I. and Flury, F., 1994. Hydrogeological investigation of porous environments by radio magnetotelluric-resistivity (RMT-R 12-240 kHz). *J. Appl. Geophys.*, **31**(1-4), 133-143.

Vozoff K. and Jupp D.L.B., 1975. Joint inversion of geophysical data. *Geophys. J. R. astr. Soc.*, **42**(3), 977-991.

Wang, S., Malehmir, A. and Bastani, M., 2016. Geophysical characterization of areas prone to quick-clay landslides using radio-magnetotelluric and seismic methods. *Tectonophysics*, **677**, 248-260.

Wang, S., Kalscheuer T., Malehmir, A., Bastani, M., Pedersen L.B., Dahlin T. and Meqbel N., 2017a. Joint inversion of lake-floor electrical resistivity tomography and boat-towed radio-magnetotelluric data illustrated on synthetic data and an application from the Äspö Hard Rock Laboratory site, Sweden. *Geophys. J. Int. (under revision)*.

Wang, S., Bastani, M., Kalscheuer, T., Malehmir, A. and Dynesius, L., 2017b. Controlled Source Boat-towed Radio-magnetotellurics for Site Investigation at Äspö Hard Rock Laboratory, Southeastern Sweden. *In 79th EAGE Conference and Exhibition 2017*, Paris.

Wikberg, P., Gustafson, G., Rhén, I. and Stanfors, R., 1991. *Äspö hard rock laboratory. Evaluation and conceptual modelling based on the pre-investigations 1986-1990* (No. SKB-TR-91-22), Swedish Nuclear Fuel and Waste Management Co..

Xiong, B. and Wang, S.G., 2011. Wave-Number Domain Features of Primary Field of H− Hz Arrangement Wide Field Electromagnetic Method. *In International Conference on Instrumentation, Measurement, Circuits and Systems* (ICIMCS 2011). ASME Press.

Xu, S., 1994. *The finite element method in geophysics*. Science Press.

Zhang, Y. and Key, K., 2016. MARE3DEM: A three-dimensional CSEM inversion based on a parallel adaptive finite element method using unstructured meshes. In *SEG Technical Program Expanded Abstracts 2016*, 1009-1013. Society of Exploration Geophysicists.

Zhang, P., Roberts, R.G., Pedersen L.B., 1987. Magnetotelluric strike rules. *Geophysics*, **52**(3), 267-278.

Acta Universitatis Upsaliensis

Digital Comprehensive Summaries of Uppsala Dissertations from the Faculty of Science and Technology 1536

Editor: The Dean of the Faculty of Science and Technology

A doctoral dissertation from the Faculty of Science and Technology, Uppsala University, is usually a summary of a number of papers. A few copies of the complete dissertation are kept at major Swedish research libraries, while the summary alone is distributed internationally through the series Digital Comprehensive Summaries of Uppsala Dissertations from the Faculty of Science and Technology. (Prior to January, 2005, the series was published under the title "Comprehensive Summaries of Uppsala Dissertations from the Faculty of Science and Technology".)

Distribution: publications.uu.se
urn:nbn:se:uu:diva-327096

ACTA
UNIVERSITATIS
UPSALIENSIS
UPPSALA
2017